Journal of Neuro-Oncology (2026) 177:16
https://doi.org/10.1007/s11060-025-05416-z

RESEARCH

Phosphoenolpyruvate carboxykinase 2 as a prognostic biomarker: expression and clinical significance in Group 3 and Group 4 medulloblastoma

Shiqi Zheng[1] · Long Lin[2] · Guotao Ren[1] · Hangzhu Lan[1] · Yingying Pan[1] · Meng Zhang[1] · Wenbin Guan[1] · Ruifen Wang[1] · Lifeng Wang[1]

Received: 11 November 2025 / Accepted: 29 December 2025

Abstract

Purpose Despite Phosphoenolpyruvate carboxykinase 2 (PCK2) has attracted growing attention as a potential biomarker in cancer research, its role in medulloblastoma (MB) remains unclear. This research aims to evaluate PCK2 as a novel biomarker for groups 3 and 4 MB and to investigate its associations with prognosis and the tumor immune microenvironment.

Methods Five cohorts were extracted to identify characteristic genes associated with MB molecular subtypes through gene differential expression analysis and machine learning techniques. Kaplan-Meier survival analysis, alongside univariate and multivariate COX regression analyses, was employed to investigate the relationship between *PCK2* expression and clinical significance. Immunohistochemistry was used to detect *PCK2* expression in MB samples. ROC analysis was performed to verify the specificity of *PCK2*. MCP-counter, CIBERSORT, and ssGSEA were used to explore the correlation of tumor-infiltrating immune cells according to *PCK2* expression. Immunofluorescence was performed to testify the co-expression patterns across PCK2, CD206 and PD-L1 in MB tissues.

Results *PCK2* is increasingly expressed in Group 3 MB and could serve as an independent poor prognostic indicator for MB patients. *PCK2* correlates with immune infiltrates and immunosuppression. Furthermore, *PCK2* exhibits a positive correlation with M2-type macrophage infiltration and is co-expressed with CD206 and PD-L1 in MB tissues.

Conclusion Our study demonstrates that PCK2 may serve as a reliable biomarker for differentiating Group 3 from Group 4 MB and could potentially play a role in immunotherapy-related mechanisms.

Keywords Medulloblastoma · PCK2 · Immunohistochemical staining · Immune infiltration · Prognosis

Abbreviations

MB	Medulloblastoma
GEO	Gene Expression Omnibus
WHO	World health organization
SYN	Synaptophysin
NeuN	Neuronal Nuclei
GFAP	Glial Fibrillary Acidic Protein
INI-1	Integrase Interactor 1
Lin28A	Lin-28 Homolog A
EMA	Epithelial Membrane Antigen
C	Classic
DN	Desmoplastic/nodular
LC/A	Large cell/anaplastic Medulloblastoma
MBEN	MB with extensive nodularity

Shiqi Zheng and Long Lin contributed equally to this work.

✉ Lifeng Wang
wanglifeng@xinhuamed.com.cn

Shiqi Zheng
zsq2386130885@163.com

Long Lin
liong0227@163.com

[1] Department of Pathology, Xinhua Hospital Affiliated to Shanghai Jiao Tong University School of Medicine, Shanghai, China

[2] Department of Radiation Oncology, Clinical Oncology School of Fujian Medical University Fujian Cancer Hospital, (Fujian Branch of Fudan University Shanghai Cancer Center), Fujian Cancer Hospital, Fuzhou, China

Published online: 25 February 2026

Introduction

Medulloblastoma (MB) is the most common embryonal brain tumor in children, accounting for 20% of pediatric central nervous system tumors. Its incidence is 0.18 per 100,000, with a male-to-female ratio of approximately 1.7:1 and a median age at diagnosis of 9 years [1]. According to the 2021 5th edition of the WHO Central Nervous System Tumors classification, MB molecular subtypes are categorized into four groups: WNT-activated, SHH-activated, Group 3 and Group 4 [2]. The prognosis varies significantly among subtypes. Group 3 MB exhibits the poorest overall prognosis and often necessitates a more aggressive treatment regimen. Currently, DNA methylation serves as the "gold standard" for molecular typing of MB. However, the high costs associated with detection and limited technical accessibility have hindered its widespread clinical adoption. There remains a deficiency of effective biological markers for distinguishing between Group 3 and Group 4 MB. Consequently, there is an urgent need to identify novel biomarkers that are both highly accessible and demonstrably effective in aiding the preliminary clinical classification of MB.

Metabolic reprogramming constitutes one of the fundamental characteristics of cancer [3]. Tumor cells typically possess an enhanced capacity for synthesizing energy and biological macromolecules, and they can also modify the surrounding microenvironment to fulfill their proliferative demands. This metabolic pattern is influenced by various factors, including nutrient availability, oxygen levels, and genetic variations, which in turn dictate the differentiated utilization of energy sources such as glucose and fatty acids [4]. In contrast to normal tissue cells, most cancer cells predominantly rely on the glycolytic pathway for rapid energy production, a phenomenon known as the Warburg effect [5]. This process not only facilitates the malignant proliferation of tumors but also contributes to their resistance to chemotherapy. Furthermore, the metabolic reprogramming of the tumor microenvironment (TME) is intricately linked to tumor immune evasion [6].

Phosphoenolpyruvate carboxykinase 2 (PCK2) serves as a crucial rate-limiting enzyme in the glycolytic and gluconeogenic pathways [7–9]. Its functions extend beyond the traditional regulatory roles associated with these pathways, significantly contributing to metabolic reprogramming in tumors [10]. In recent years, *PCK2* has emerged as a focal point of research within the field of oncology. *PCK2* plays a central regulatory role in the initiation and progression of various malignant tumors, including hepatocellular carcinoma, breast cancer, and lung cancer [11]. It influences tumor progression and patient prognosis through multiple mechanisms and may be linked to tumor-associated immunosuppressive states [12–14].

In recent years, advancements in technologies such as machine learning (ML) and single-cell sequencing have facilitated the exploration of the molecular regulatory mechanisms underlying tumors and the identification of biomarkers with clinical translational potential [15–18]. Here, we integrated multi-cohort data from online dataset, developed a prediction model for Group 3 and Group 4 MB using ML techniques, and identified the key gene *PCK2*. We also revealed the prognostic value and mechanism of action of *PCK2* in MB from multiple perspectives, which provided a theoretical basis for the development of therapeutic strategies targeting the *PCK2*-associated immune microenvironment.

Methods and materials

Gene expression data from public databases

Gene expression data and clinical information from a total of 1676 MB patients were obtained from the Gene Expression Omnibus (GEO, http://www.ncbi.nlm.nih.gov/geo/) and R2 Genomics Analysis and Visualization Platform (http://r2.amc.nl). Five RNA-seq datasets with molecular sub types were included: GSE37418, GSE85217, emtab10767, mbffpe420, and mbffpe86. The "limma" package in the R software (Version 4.3.2) was used to normalize and standardize the datasets. And the "ComBat" method within the "sva" package was applied to mitigate batch effects across all datasets, followed by pooling the five datasets. Principal component analysis (PCA) demonstrated that batch effects were eliminated in all datasets.

Inclusion and exclusion criteria

All samples included in our study met the following inclusion criteria: ① Pathologically confirmed diagnosis of MB; ② Molecular subtypes of all MB samples as Group 3 MB ($n=401$) or Group 4 MB ($n=792$). Exclusion criteria included: The molecular subtype is uncertain or of other types ($n=483$).

Screening for MB molecular subtype-associated feature genes

With filtering criteria of LogFC > 1 and $p<0.05$, differential gene expression analysis was performed on the included data using the "limma" package. The "pheatmap" package facilitated the creation of a heatmap. Three ML algorithms, Least Absolute Shrinkage and Selection Operator (LASSO),

Support Vector Machine with Radial Basis Function Kernel (SVM-RFE), and Random Forest (RF), were applied to identify feature genes associated with molecular subtypes. The "ggvenn" and "ggplot2" package were utilized to generate a Venn plot and a volcano plot respectively, enabling the visualization of the results.

Construction of MB molecular subtyping prediction models

The merged dataset was randomly divided into a training set (70.0%) and a validation set(30.0%). Ten ML algorithms were used to construct models for diagnosing MB molecular subtypes: Partial Least Squares (PLS), Gradient Boosting with Generalized Linear Models as base learners (glmboost), RF, SVM-RFE, Decision Tree (DTS), Gradient Boosting Machine (GBM), k-Nearest Neighbors (KNN), eXtreme Gradient Boosting (XGBoost), Neural Network (nnet), and Logistic Regression (LogisticR). Cross-validation was performed using the "repeatedcv" method, and model performance was evaluated through receiver operating characteristic (ROC) curve analysis.

The SHapley Additive exPlanations (SHAP) method was utilized to identify and analyze the key feature genes associated with MB molecular subtypes. By quantifying the contribution of each feature to the model's predictions, the maximum likelihood model is elucidated using SHAP [19]. The "fastshap" and "shapviz" packages were used to compute the mean Shapley value for each gene within the training and validation cohorts of each model [20]. Genes exerting a significant influence on the models were filtered for further analysis.

Clinical MB samples

All paraffin samples, clinicopathological information, and follow-up data were obtained from the Department of Pathology at Xinhua Hospital Affiliated to Shanghai Jiao Tong University School of Medicine between 2012 and 2024 ($n=264$). Two senior pathologists independently assessed hematoxylin-eosin-stained sections using a blinded approach and classify tumors into four histological subtypes: Classic MB, Desmoplastic/nodular MB, MB with extensive nodularity, and Large cell/anaplastic MB. All research methods adhered to the ethical principles of the Declaration of Helsinki, the International Code of Ethics for Human Health Research, and other established medical ethics standards. Approval was obtained from the Ethics Committee of Xinhua Hospital Affiliated to Shanghai Jiao Tong University School of Medicine. (Ethics Approval Number: XHEC-D-2025-181).

DNA methylation profile analysis and molecular subtyping

Genomic DNA from tumor tissues was extracted using a kit (Qiagen) and subjected to quality control. Qualified DNA samples underwent bisulfite conversion using the EZ DNA Methylation-Gold Kit (Zyme Research). Converted DNA was analyzed using the Illumina Infinium MethylationEPIC v2.0 (or 850 K) array for whole-genome methylation profiling, simultaneously assessing methylation status at over 850,000 CpG sites. Experimental procedures were strictly followed according to the manufacturer-provided standard protocols. Raw data (IDAT files) underwent preprocessing in R software using the "minfi" package, including background correction, probe type bias correction, and normalization. After removing low-quality probes with detection p-values >0.01 and cross-reactive probes, a β-value matrix was obtained for each CpG site. Final molecular subtyping was performed by submitting the preprocessed data to the online medulloblastoma methylation classifier developed by the German Cancer Research Center (DKFZ). This classifier assigns subtypes by calculating similarity scores between samples and reference subtypes (WNT, SHH, Group 3, Group 4). A calibration score ≥ 0.9 was considered indicative of a reliable subtyping result.

Immunohistochemical staining

The tissues were fixed in 3.7% neutral buffered formalin, dehydrated, and paraffin-embedded. Sections were cut to a thickness of 4–5 μm. Immunohistochemistry (IHC) was conducted using the EnVision method with primary antibody PCK2 (1:100, 14892-1-AP, Proteintech). The procedures adhered to the kit instructions, employing the Leica fully automatic staining system and the Roche Ventana Ultra fully automatic immunohistochemical staining instrument. Two pathologists randomly selected at least 5 high-power fields (× 400) to evaluate PCK2 staining. Intensity scoring criteria: 0 (negative), 1 (weak), 2 (moderate), 3 (strong). Percentage of positive cells scoring criteria: 1 (1–25%), 2 (26–50%), 3 (51–75%), 4 (76–100%). The final immunoreactivity score (IRS) of 0–12 was obtained by multiplying the intensity and percentage scores [21].

To identify the optimal cutoff value for *PCK2* expression, log-rank tests were performed on all potential cutoff values with non-zero scores, yielding corresponding chi-square values and p-values. The screening criteria stipulated that each group must have a sample size of at least 10 and that the chi-square value should be maximized. PCK2 IHC score of 8 points was established as the optimal cutoff value. And patients were categorized into a high expression group (IRS ≥ 8 points) and a low expression group (IRS <8

points). Furthermore, the ROC curve was generated using the "pROC" package to assess the predictive efficacy of the IHC score for Group 3 and Group 4 MB.

Survival analysis and statistical methods

The "survminer" package facilitates the calculation of the optimal cutoff value via the surv_cutpoint function, which is based on maximally selected rank statistics. All patients with MB were categorized into the high *PCK2* expression group and the low *PCK2* expression group according to the optimal cutoff value. Kaplan-Meier analysis was performed using the "survival" and "survminer" packages, resulting in the plotting of survival curves. Univariate and multivariate Cox regression analyses were executed with the "survival" package. The intensity and direction of associations in both univariate and multivariate models were quantified by calculating the hazard ratios (HRs) and their corresponding 95% confidence intervals (CIs), with forest plots generated using the "ggplot2" package. The Pearson test and Mann-Whitney U test were employed to assess the correlation of variables and to mitigate multicollinearity interference. Patients without overall survival (OS) data were excluded from the analysis, and the p-value of <0.05 was deemed statistically significant.

The comparison of clinical and pathological data was conducted using R software (version 4.3.2). The correlation test was performed using a completely random chi-square test. Statistical significance was determined using a significance level of $p<0.05$.

Functional analysis

Based on the logFC values derived from the comparison of the high *PCK2* expression group with the low expression group, all genes in the combined dataset were ranked. The "clusterProfiler" package was employed to perform enrichment analysis on the sorted genes. The Homo sapiens gene set corresponding to "c2.cp.kegg.hs.symbols.gmt" was downloaded from the Molecular Signatures Database (http://www.gsea-msigdb.org/). The criteria for enrichm ent results were established as a $p<0.05$ and a false discovery rate (FDR)<0.25. The results of the enrichment analysis were visualized using the "enrichplot" package. Gene set variation analysis (GSVA) was conducted on the aforementioned gene sets utilizing the "GSVA" package to obtain enrichment scores for each sample across the pathways. The enrichment scores were normalized to a range of 0–1, and pathways with minimal variance were excluded based on the criterion of standard deviation (standard deviation>0.01). The functional differences among the enriched pathways post-filtering were analyzed using the "limma" package, and a bar chart was generated with the "ggpubr" package to visualize the results of the differential pathways. The evaluation of the association between *PCK2* expression levels and the biological functions and signaling pathways related to the molecular classification of MB was conducted.

Immune infiltration analysis

The analysis of immune infiltration within the RNA-seq dataset was performed utilizing three algorithms: Microenvironment Cell Populations-counter (MCP-counter), Cell-type Identification By Estimating Relative Subsets Of RNA Transcripts (CIBERSORT), and Single-sample Gene Set Enrichment Analysis (ssGSEA). The "MCPcounter" package was employed to compute the absolute abundance scores for ten major immune cell types, including T cells, CD8+T cells, cytotoxic lymphocytes, natural killer cells, B cell lines, monocyte lines, myeloid dendritic cells, neutrophils, endothelial cells, and fibroblasts. To assess the variations in immune cell infiltration across different expression groups of *PCK2*, a violin plot was generated using "ggpubr" to effectively visualize the findings. The "cibersort" package was employed to analyze immune cell infiltration within the gene expression data. Differences in immune cell infiltration levels between high *PCK2* expression and low *PCK2* expression were assessed. The relative abundance of 22 immune cell types in each sample was quantitatively analyzed, and the correlation between *PCK2* and these immune cells was examined. Results were visualized through box plots generated using the "ggpubr" package. The ssGSEA scores for each sample across 29 immune functions were calculated to investigate the differences in immune functions between the high *PCK2* expression and low *PCK2* expression, with results also visualized via box plots created using the "ggpubr" package. The correlation between *PCK2* and immune checkpoint-related genes was analyzed using Pearson correlation analysis, and the "corrplot" package was utilized to generate a correlation heatmap.

Immunofluorescent staining

Standard immunofluorescence method was used to stain paraffin section samples. Anti-PCK2 antibody (1:400, 14892-1-AP, Proteintech), anti-PD-L1 antibody (1:200, R013735, Epizyme) and anti-CD206 antibody (1:500, 24595T, Cell Signaling Technology) were used. Fluorescence staining was performed using HRP goat anti-rabbit-mouse universal secondary antibody (ready-to-use, RCB054, Shanghai Recordbio Biological Technology Co., Ltd.) and HRP goat anti-rabbit secondary antibody (ready-to-use, RCA054, Shanghai Recordbio Biological Technology Co., Ltd.). The secondary antibodies were pre-diluted to the optimal

working concentration by the manufacturer and required no further dilution. The main steps included: the sections were dewaxed by xylene, hydrated with gradient ethanol, subjected to heat-mediated antigen repair (EDTA, pH 9.0) and cooled naturally. Subsequently, endogenous peroxidase was blocked using 3% H_2O_2 and 3% BSA was blocked for 10 min at room temperature. The primary antibody working solution was added dropwise to the sections and incubated overnight at 4 °C away from light. On the following day, after sufficient washing with PBS, the fluorescent labeled secondary antibody of the corresponding species was added dropwise and incubated for 1 h at room temperature away from light. Finally, the nuclei were restained using DAPI and the sections were sealed with an anti-fluorescence quenching sealer. The slices were subjected to multi-channel image acquisition under a fluorescence scanner, and the co-localization signals were quantitatively analyzed and visualized using ImageJ software.

Results

Data pre-processing

A total of 1,193 MB samples from public databases were analyzed, which included 525 samples from GEO (GSE85217 and GSE37418), as well as 668 samples from R2 Genomics Analysis and Visualization Platform (emtab10767, mbffpe420, and mbffpe86). The clinicopathological characteristics of MB patients included in the five datasets are detailed in Table S1. The PCA results, both before and after batch correction (Fig. S1A-B), indicate that the batch effect in the combined dataset has been effectively eliminated.

Machine learning-based screening of key genes for MB molecular subtyping

383 differentially expressed genes (DEGs) associated with molecular subtypes were identified from the merged dataset (Fig. 1A). Five candidate genes (*PCK2*, *RBM24*, *PTPN5*, *SIPA1L2*, and *BARHL1*) were selected based on the intersection of three ML algorithms (LASSO, SVM-RFE, and RF) (Fig. S2) to construct a molecular subtype prediction model (Fig. 1B-C). The dataset was randomly divided into a training set (70.0%) and a validation set (30.0%). Ten machine learning models were constructed based on the training set, and their performance was validated on the validation set. The predictive efficacy of each model for MB molecular subtypes was evaluated using the area under the receiver operating characteristic curve (AUC), with the XGBoost model demonstrating optimal predictive performance (AUC = 0.988) (Fig. 1D). The SHAP algorithm was employed to elucidate the prediction mechanism of the XGBoost model (Table S2). The SHAP integrated visualization diagram distinctly illustrated the contribution of each candidate gene to the model's prediction outcomes. Notably, *PCK2* emerged as a core characteristic gene influencing the model's predictions (Fig. 1E-F). The Kruskal-Wallis rank test ($p = 0.222$) indicated no significant difference in expression among the groups, while the average coefficient of variation of *PCK2* expression across the five combined datasets (Average CV = 0.252) suggested robust expression stability, indicating that *PCK2* exhibits a consistent expression trend across different datasets (Fig. S3A-B), solidifying its role as a key gene for predicting MB molecular subtypes.

PCK2 is highly expressed in MB and correlates with shorter OS

The optimal expression cutoff value for *PCK2* (cutoff value = 2.48) in the MB mRNA expression cohort was established using the log-rank test (Fig. 2A). Based on the threshold, MB patients were divided into high *PCK2* expression and low *PCK2* expression group. Kaplan-Meier survival analysis indicated that MB patients exhibiting high *PCK2* expression had a significantly poorer prognosis and a markedly reduced OS compared to those with low *PCK2* expression (log-rank test, $p < 0.001$) (Fig. 2B).

Survival analysis based on the expression of *PCK2* was performed in conjunction with clinicopathological characteristics, including age, gender, molecular typing, histological typing, and M stage. The Kaplan-Meier curve demonstrated a significant association between *PCK2* expression and patient prognosis. In the subgroup analysis, only the subgroups with age ≤ 3 years ($p = 0.147$) and histological typing of LC/A ($p = 0.401$) did not show significant results. In contrast, all other subgroups, encompassing gender, alternative histological typing, molecular typing, and metastasis status, exhibited a significant correlation between high *PCK2* expression and poor prognosis ($p < 0.05$) (Fig. 2C-L).

The comparison of *PCK2* mRNA expression levels between Group 3 and Group 4 MB revealed that *PCK2* expression was significantly higher in Group 3 than in Group 4 ($p < 0.001$) (Fig. 2M), indicating that *PCK2* expression is closely associated with specific molecular subtypes of MB, particularly exhibiting high expression in the Group 3 MB, which is characterized by the poorest prognosis. And the analysis of *PCK2* expression across various clinicopathological features indicated that MB patients aged ≤ 3 years and those with the histological subtype LC/A exhibited significantly higher *PCK2* expression (Fig. 2N-R). The result implies that high *PCK2* expression may exacerbate the poor prognosis of patients by facilitating tumor progression.

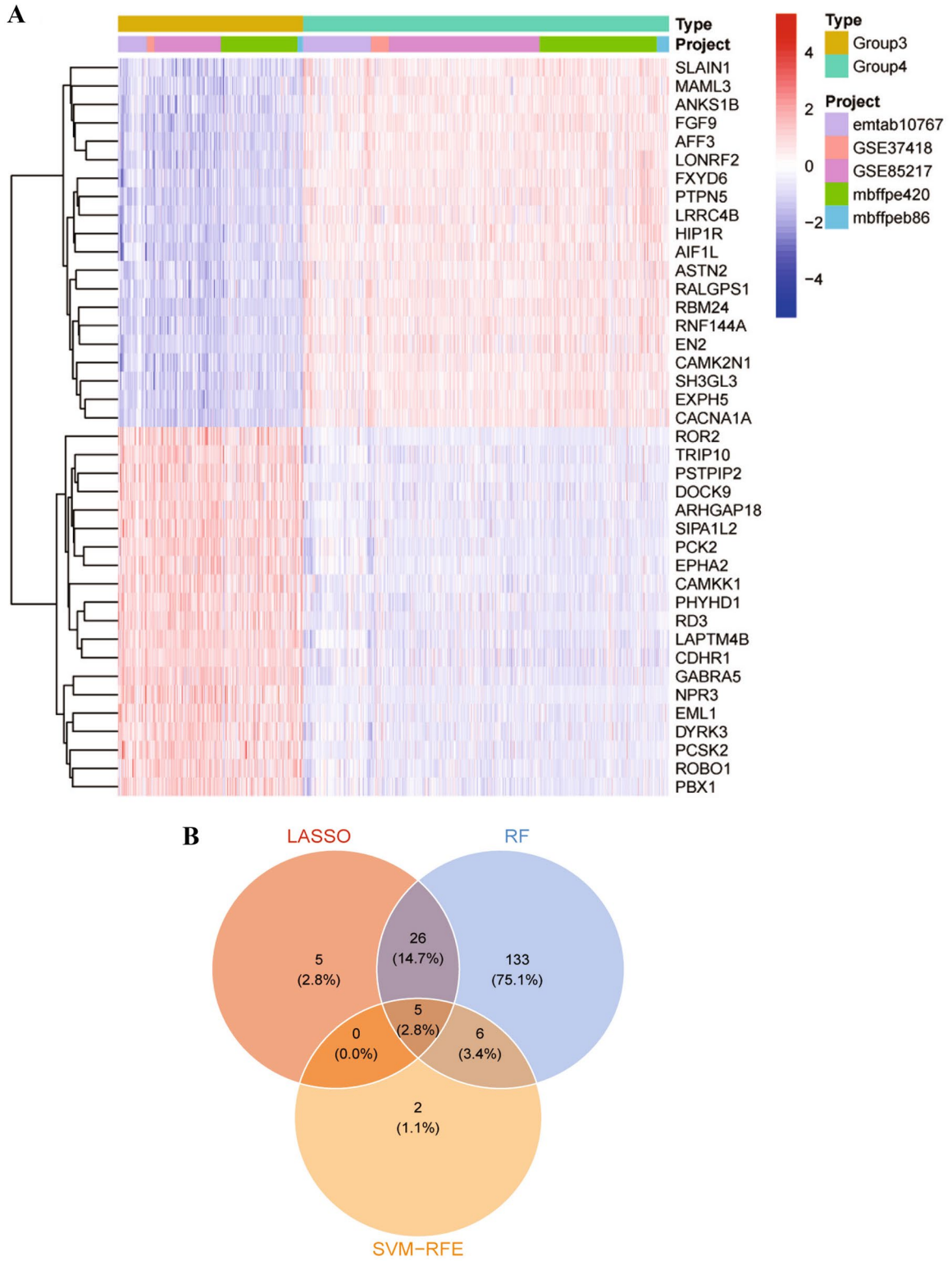

Fig. 1 Screening candidate genes for MB molecular subtyping using ML. **A** Differential expression analysis identified genes distinguishing Group 3 and Group 4 MB (the top 40 differentially expressed genes are shown); **B** Five candidate genes associated with molecular subtypes, venn diagram; **C** The differentially expressed genes between Group 3 and Group 4 MB, volcano plot; **D** ROC curves compare the performance of 10 ML models for predicting MB molecular subtypes; E-F. SHAP analysis identified key genes for subtype prediction (E: bar chart of SHAP values, F: honeycomb plot of SHAP values)

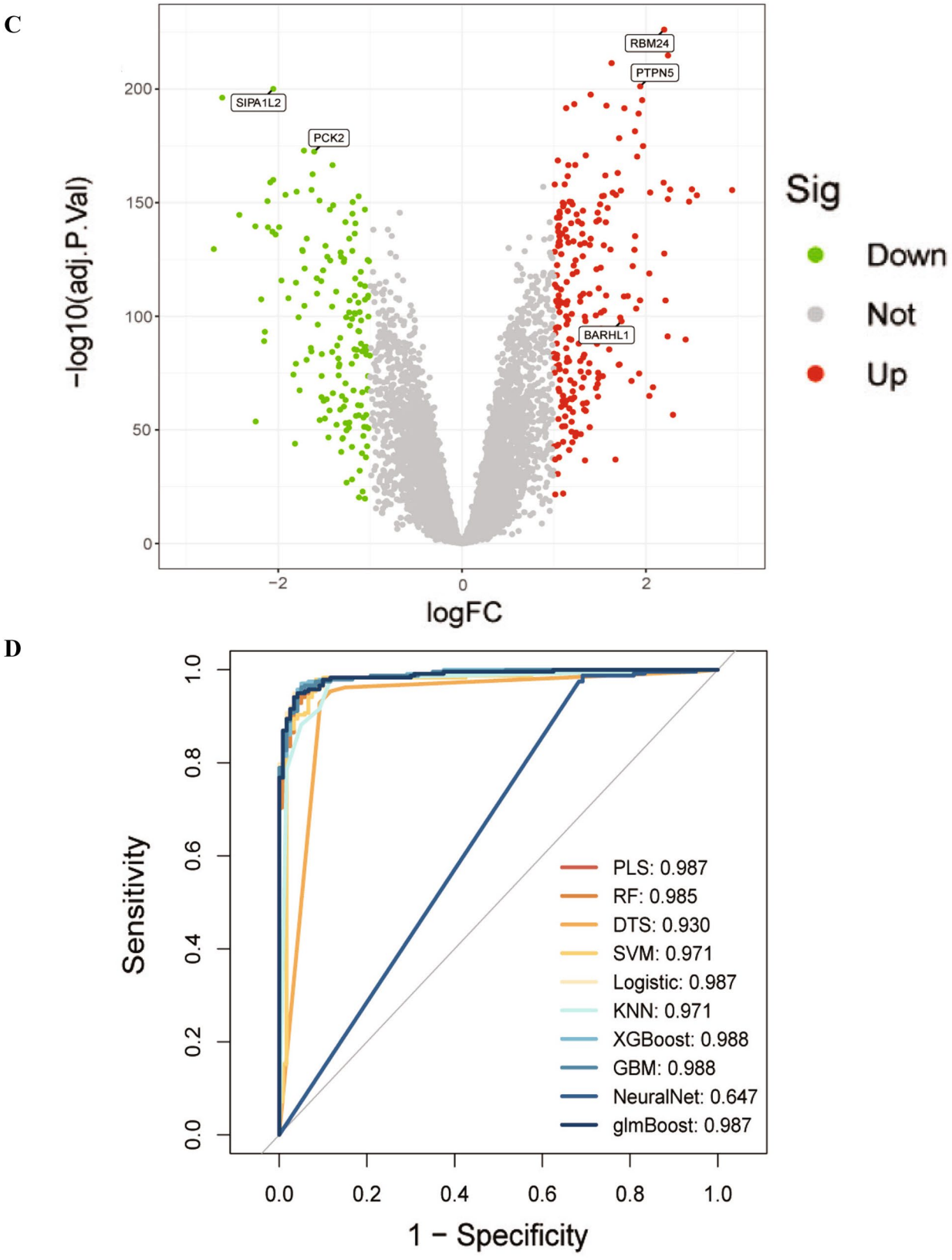

Fig. 1 (continued)

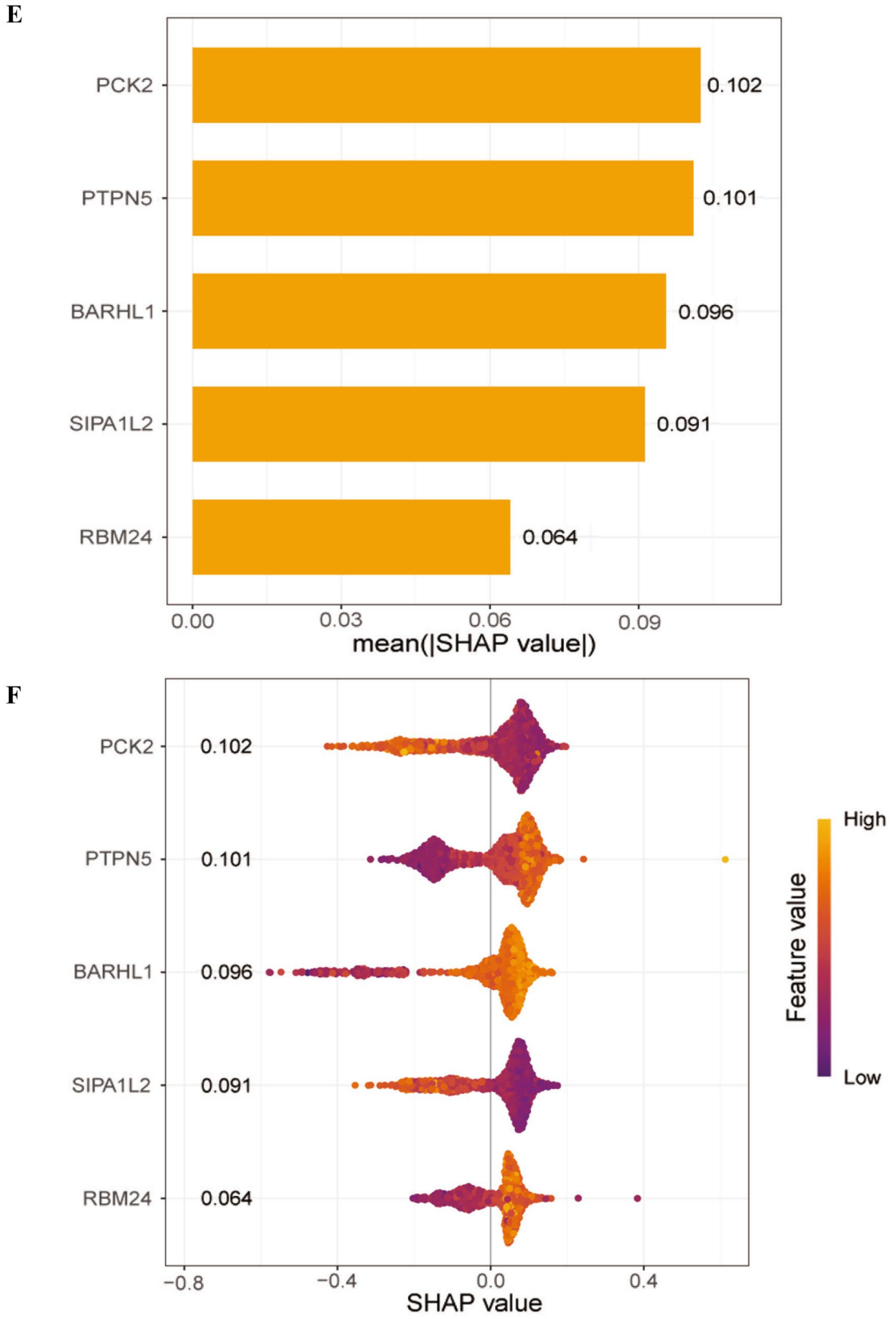

Fig. 1 (continued)

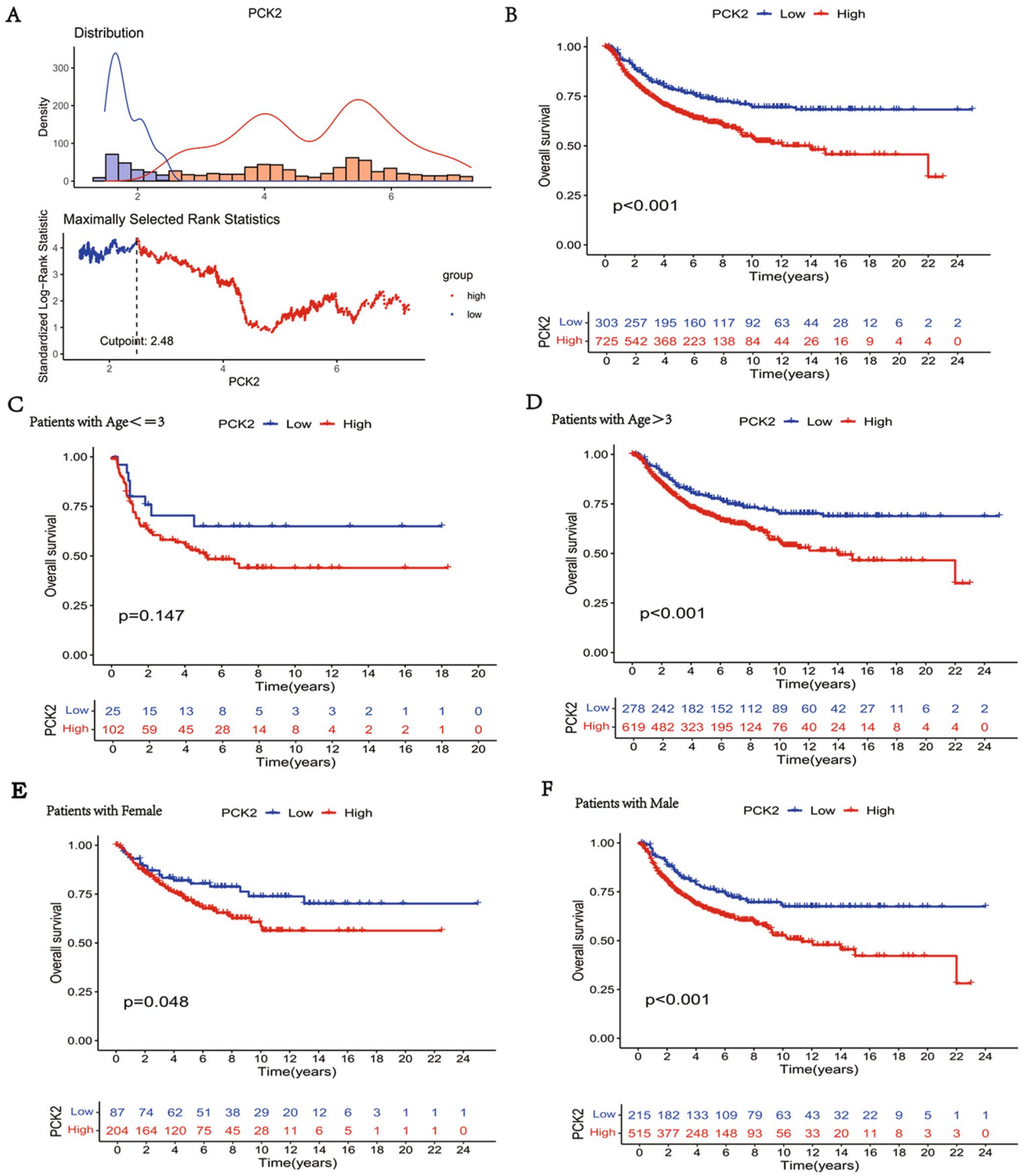

Fig. 2 The OS relation and expression of *PCK2* in MB patients, with subgroup analyses of clinicopathological parameters. **A** Determination of the optimal cut-off value for *PCK2* expression in the merged dataset; **B** Relationship between *PCK2* expression and OS in MB patients, Kaplan–Meier survival curve; **C**-**L**. The association between *PCK2* expression and OS across clinical subgroups, Kaplan–Meier survival curves; **M**. *PCK2* expression in Group 3 and Group 4 MB, box plots; **N**-**R**. *PCK2* expression across clinicopathological variables (N-Q: box plots, R: heatmap); **S**-**T**. Univariate and multivariate Cox regression analyses of *PCK2* expression and other variables in the MB dataset

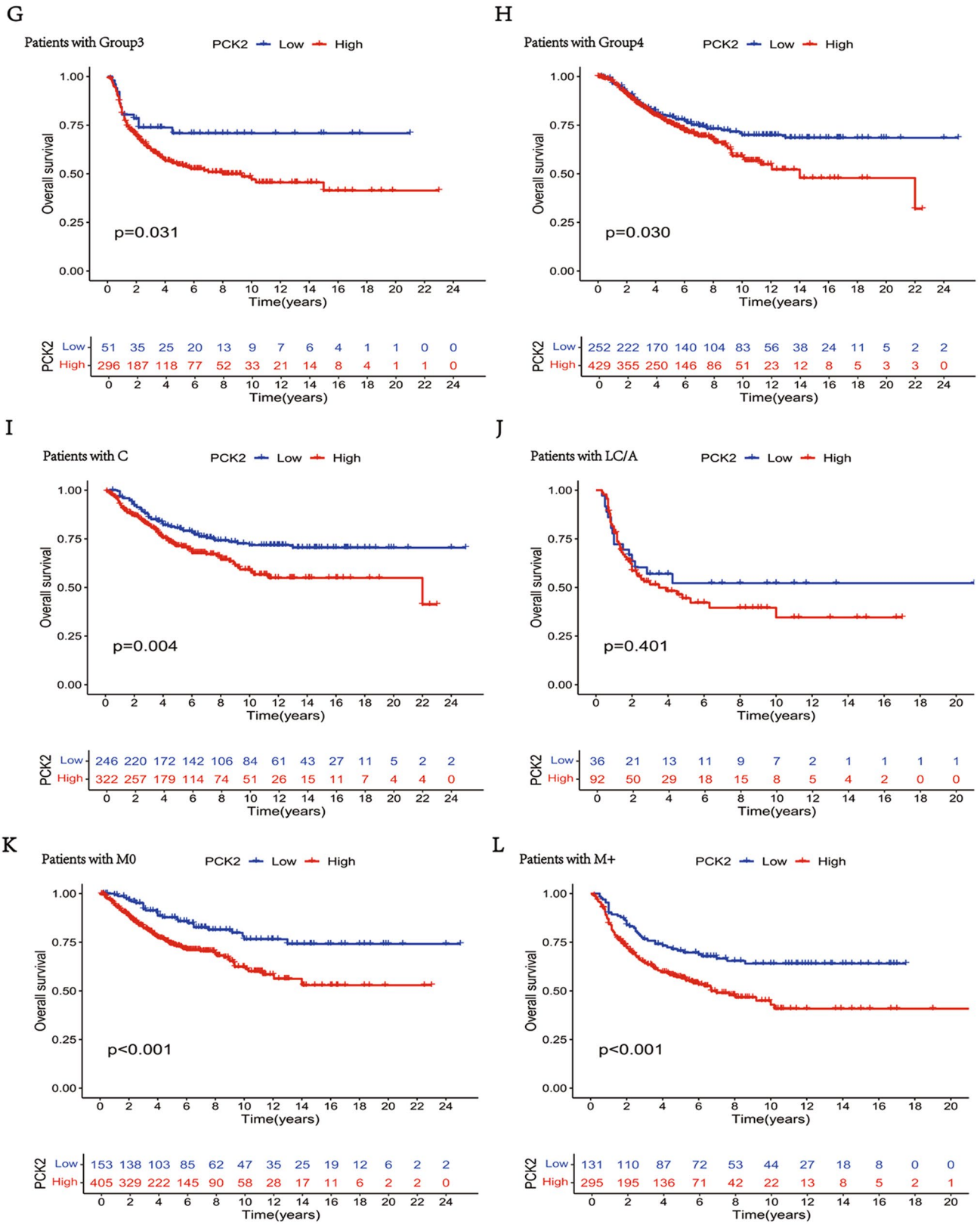

Fig. 2 (continued)

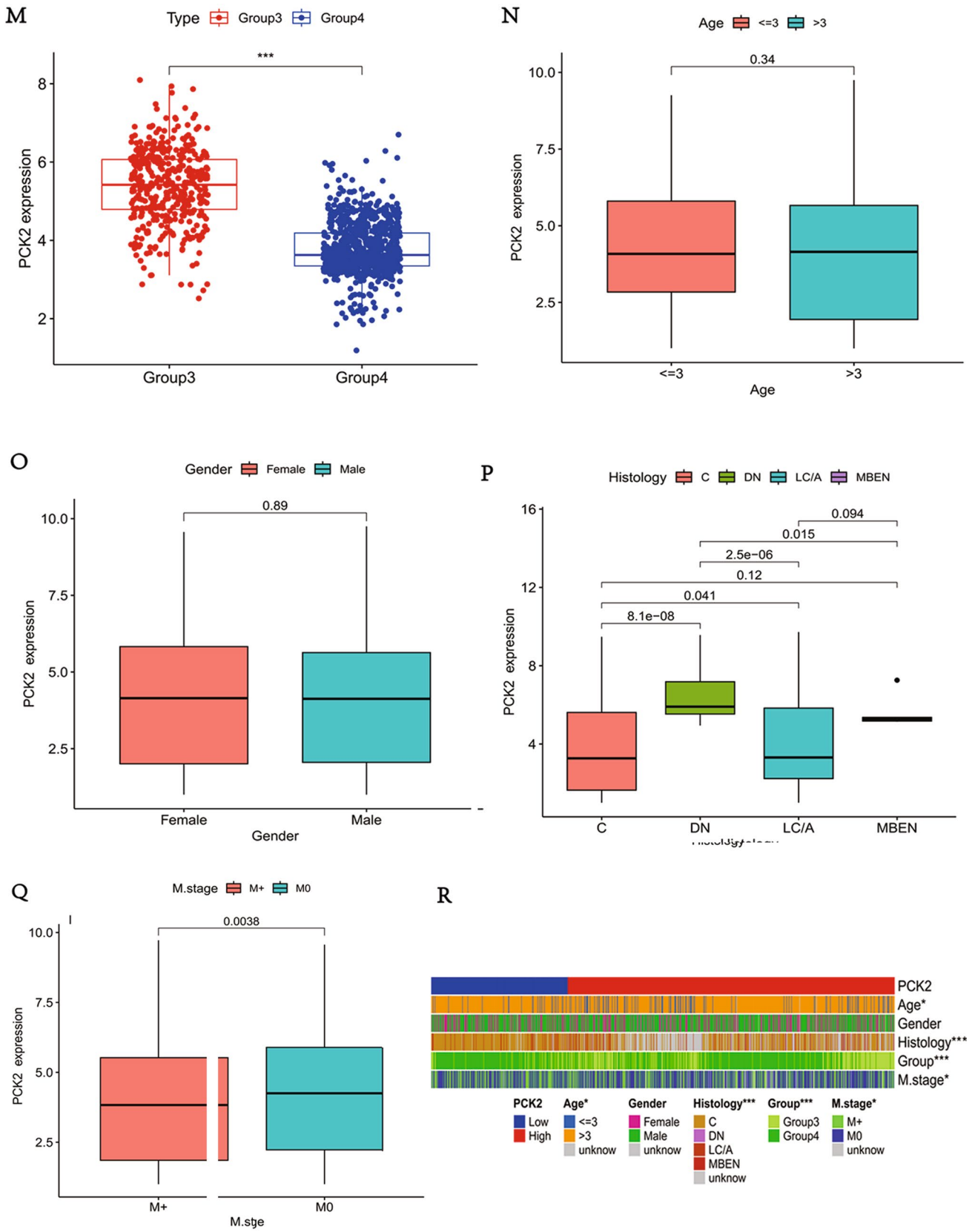

Fig. 2 (continued)

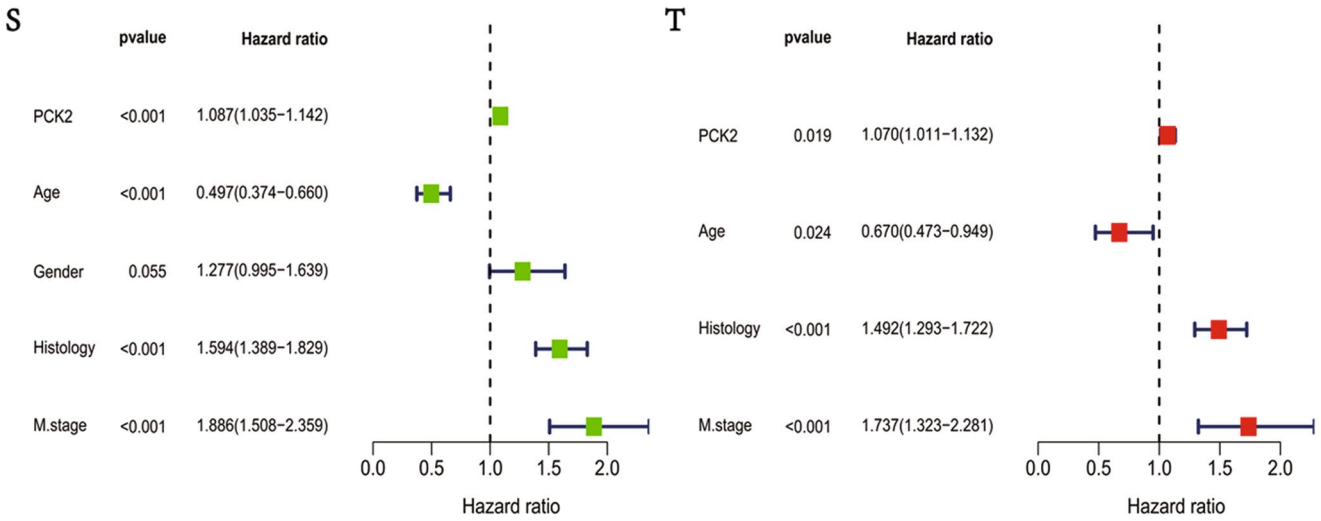

Fig. 2 (continued)

PCK2 serves as an independent prognostic biomarker in MB

The chi-square test was employed to compare the clinicopathological characteristics between low *PCK2* expression and high *PCK2* expression. There were significant differences in both histological and molecular subtypes between the two groups ($p<0.001$), demonstrating that high *PCK2* expression may be closely associated with LC/A MB and Group 3 MB, both of which are linked to adverse clinical prognostic features for MB patients.

To further explore the prognostic value of *PCK2*, univariate Cox proportional hazards regression analysis was performed using R. The analysis included clinically relevant variables such as age, gender, histological subtype, metastasis status, and *PCK2* expression. Given the significant correlation between *PCK2* expression and molecular subtypes (Mann-Whitney U test, $p<0.001$), *PCK2* was included as a core variable in subsequent modeling to avoid multicollinearity interference. The results indicated that high *PCK2* expression (HR: 1.087; 95% CI: 1.035–1.142; $p<0.001$), age≤3 years (HR: 0.497; 95% CI: 0.374–0.660; $p<0.001$), histological subtype of LC/A (HR: 1.594; 95% CI: 1.389–1.829; $p<0.001$), and metastasis (HR: 1.886; 95% CI: 1.508–2.359; $p<0.001$) were significantly associated with poor OS in MB patients (Fig. 2S). To determine whether *PCK2* functions as an independent prognostic factor, a multivariate Cox proportional hazards regression model was constructed, incorporating all significant variables. *PCK2* expression remained significantly associated with shorter OS in patients (HR: 1.070; 95% CI: 1.011–1.132; $p=0.019$), confirming that *PCK2* can serve as an independent prognostic predictor of OS in MB patients (Fig. 2T).

Clinical and pathological characteristics of MB samples

Two senior pathologists conducted a pathological review of 264 cases of MB diagnosed at the Department of Pathology, Xinhua Hospital Affiliated to Shanghai Jiao Tong University School of Medicine, between 2012 and 2024 ($n=264$). According to the histological classification criteria, 219 were Classic MB, 31 were Desmoplastic/nodular MB, 2 were MB with extensive nodularity, and 12 were Large cell/anaplastic MB (Fig. 3).

A total of 99 cases were randomly selected for DNA methylation profiling analysis to identify molecular subtypes. This cohort included 18 cases of WNT-activated MB, 26 cases of SHH-activated MB, 16 cases of Group 3 MB, and 39 cases of Group 4 MB. To ensure specificity and scientific rigor, only MB cases with clearly defined molecular subtypes of Group 3 ($n=16$) and Group 4 ($n=39$) were included (Table S3).

PCK2 immunohistochemical staining

To validate these findings, we evaluated protein expression levels in 55 human MB tissues using IHC staining. The log-rank test was employed to determine the optimal cutoff value for PCK2 IHC scores (cutoff value=8) (Fig. 4A), which enabled the stratification of patients into high-expression and low-expression groups. Subgroup distribution analysis revealed that among MB cases with high PCK2 expression, 9 cases (64.3%) were classified as Group 3 and 5 cases (35.7%) as Group 4. In contrast, among MB cases with low PCK2 expression, only 7 cases (17.1%) belonged to Group 3, whereas 34 cases (82.9%) were categorized as

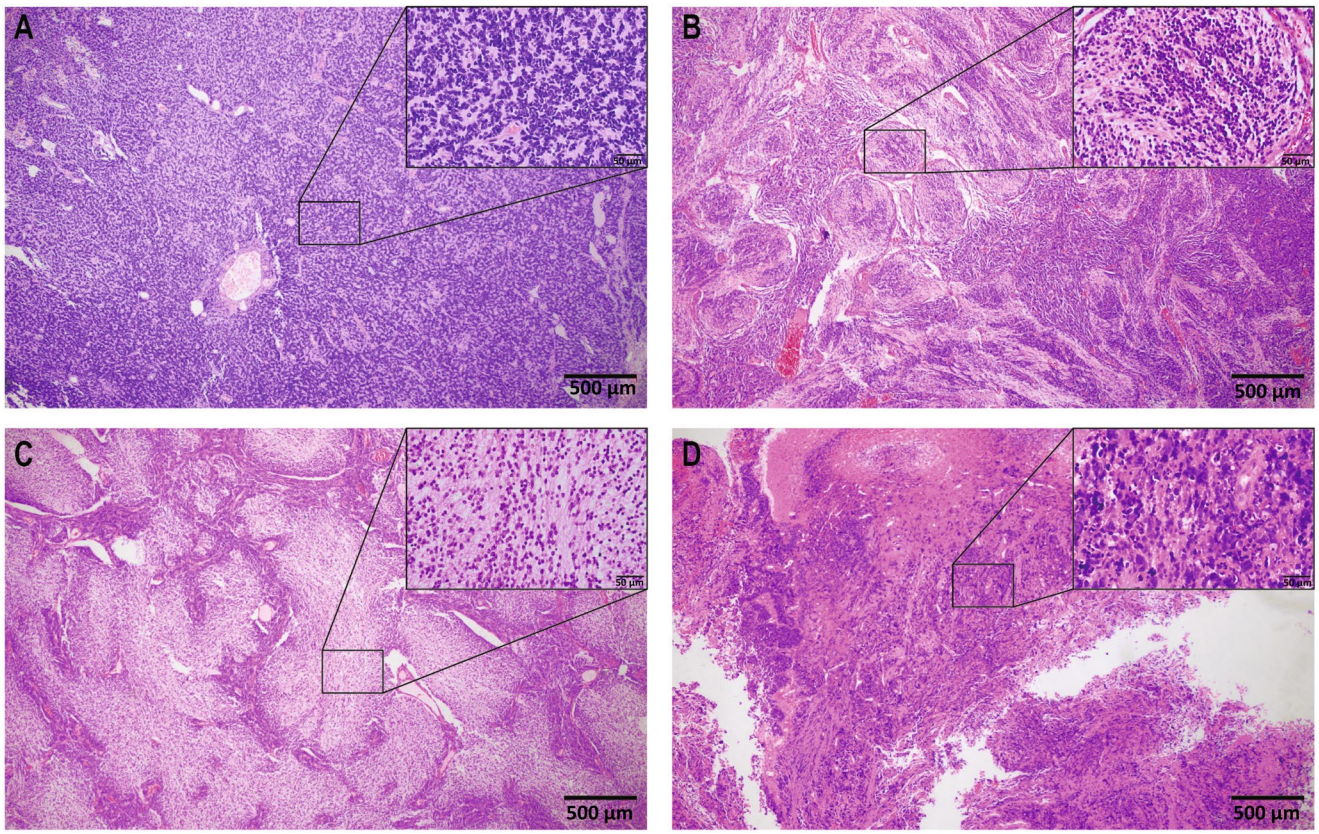

Fig. 3 Histological types of MB. **A** Classic MB (× 40); **B** Desmoplastic/nodular MB (× 40); **C** MB with extensive nodularity (× 40); **D** Large cell/anaplastic MB (× 40). (Upper right corner shows high-power field, × 400)

Group 4. The difference between two groups was statistically significant ($p<0.001$) (Fig. 4B-C). The results of the ROC curve analysis indicated that the PCK2 IHC score possessed strong discriminatory efficacy for differentiating between Group 3 and Group 4 MB (Fig. 4D), elucidating the notable heterogeneity of *PCK2* expression.

Kaplan-Meier survival analysis revealed that patients with MB exhibiting high expression of PCK2 had a significantly worse prognosis compared to those with low expression, with OS markedly reduced (log-rank test, $p=0.007$) (Fig. 4E). Time-dependent ROC analysis indicated that the predictive AUC values for *PCK2* regarding 1-year, 3-year, and 5-year OS in MB patients were 0.841, 0.880, and 0.736 respectively, demonstrating its strong predictive efficacy for survival (Fig. 4F). These findings not only confirmed the differential expression of *PCK2* across various MB subtypes but also suggested that *PCK2* overexpression may be closely associated with tumor progression and poor prognosis. Given the inherently poor prognosis of Group 3 MB, the high expression of *PCK2* in this subtype further highlights its potential as a prognostic biomarker for MB.

Correlation between *PCK2* and immune infiltration in MB

The results of GSEA and GSVA revealed that the differentially expressed genes in the high *PCK2* expression group were significantly enriched in the glycolysis and gluconeogenesis pathways ($p<0.05$). In contrast, the genes in the low *PCK2* expression group exhibited significant enrichment in the calcium signaling pathway ($p<0.05$) (Fig. 5A-C).

To investigate the regulatory role of *PCK2* in the TME of MB, three algorithms (MCP-counter, CIBERSORT, and ssGSEA) were employed. In comparison to the low *PCK2* expression group, the absolute abundance score of MCP-counter for fibroblasts in MB patients with high *PCK2* expression was significantly elevated. Conversely, in the low *PCK2* expression group, the absolute abundance scores of MCP-counter for cytotoxic lymphocytes, monocyte lineages, and neutrophils were markedly higher (Fig. 5D-G). Further analysis using CIBERSORT corroborated that *PCK2* expression exhibited a negative correlation with the relative abundance of monocytes and a positive correlation with the relative abundance of M2-type macrophages (Fig. 5H).

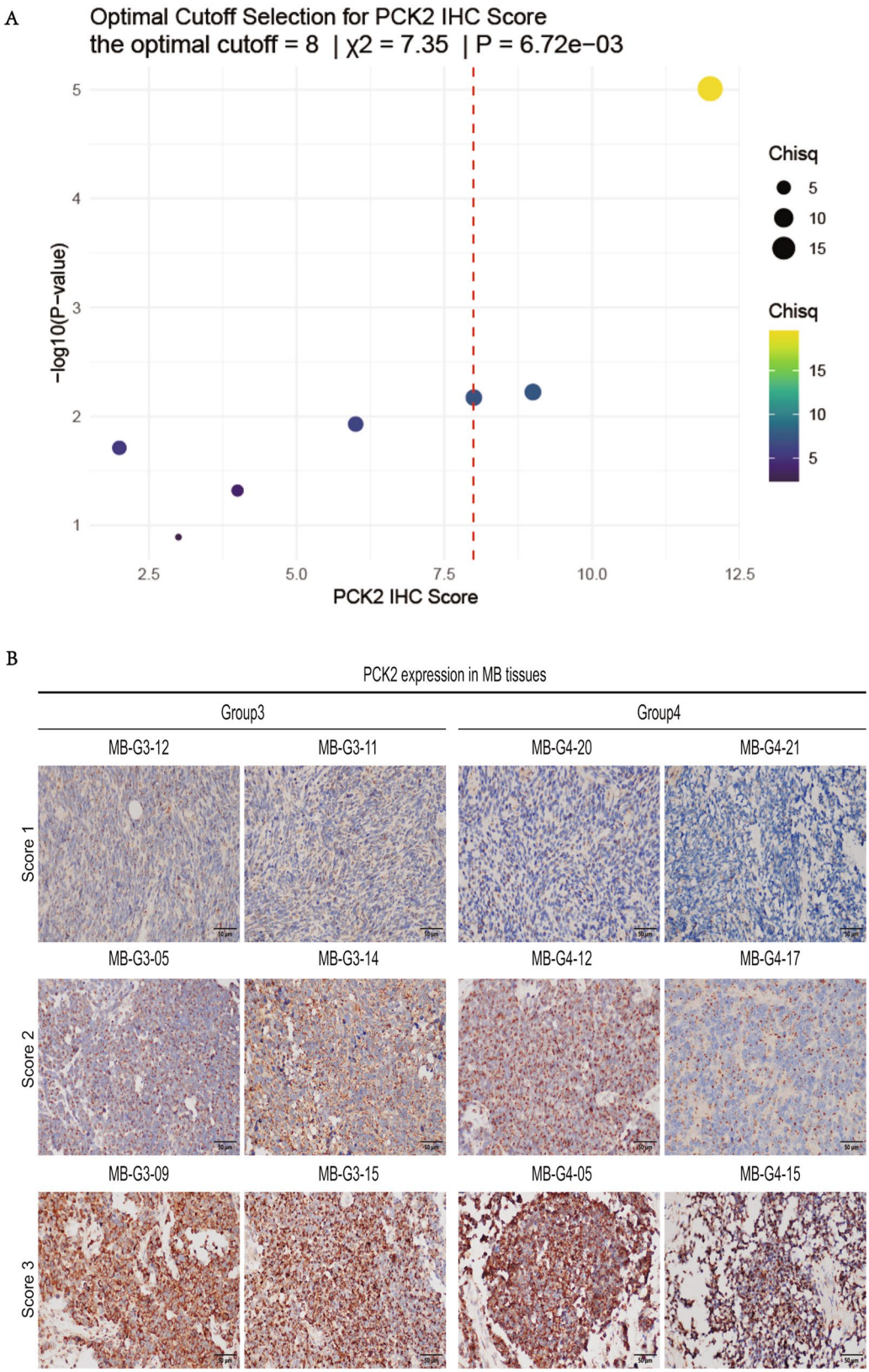

Fig. 4 IHC staining results and scoring of PCK2 in MB tissue tissues. **A** The optimal cutoff value for the PCK2 IHC score; **B** Different staining intensities of PCK2 IHC score in Group 3 and Group 4 MB (The sample ID corresponds to Table S3); **C** The differences in PCK2 IHC scores in MB samples, box plot; **D** The ability of PCK2 IHC score to predict Group 3 and Group 4 MB, ROC curve; **E** The relationship between PCK2 IHC score and OS of MB patients, Kaplan-Meier survival curve; **F** the ability of PCK2 IHC score to predict the survival of MB patients at 1-year, 3- year, and 5-year, ROC curve

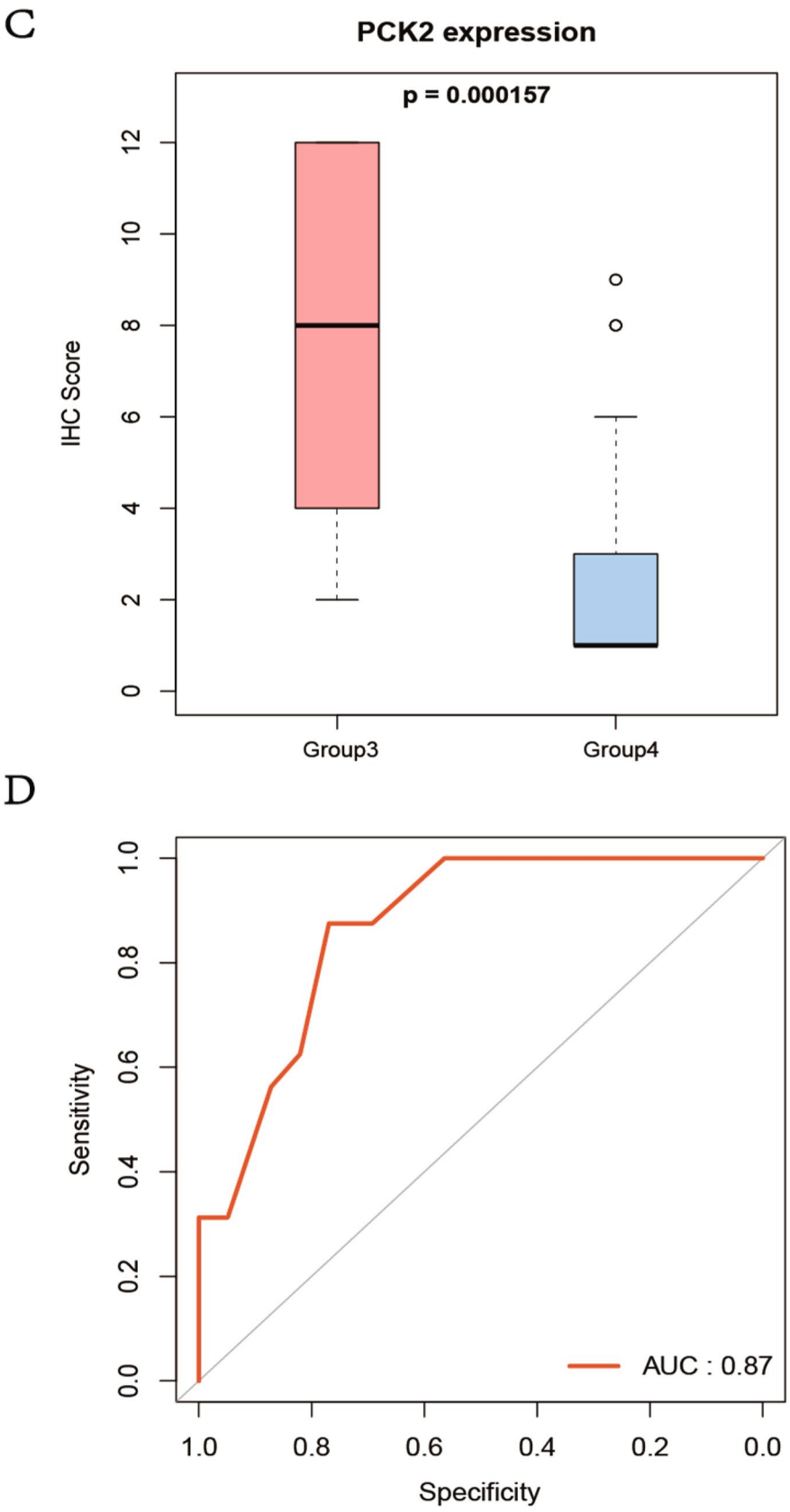

Fig. 4 (continued)

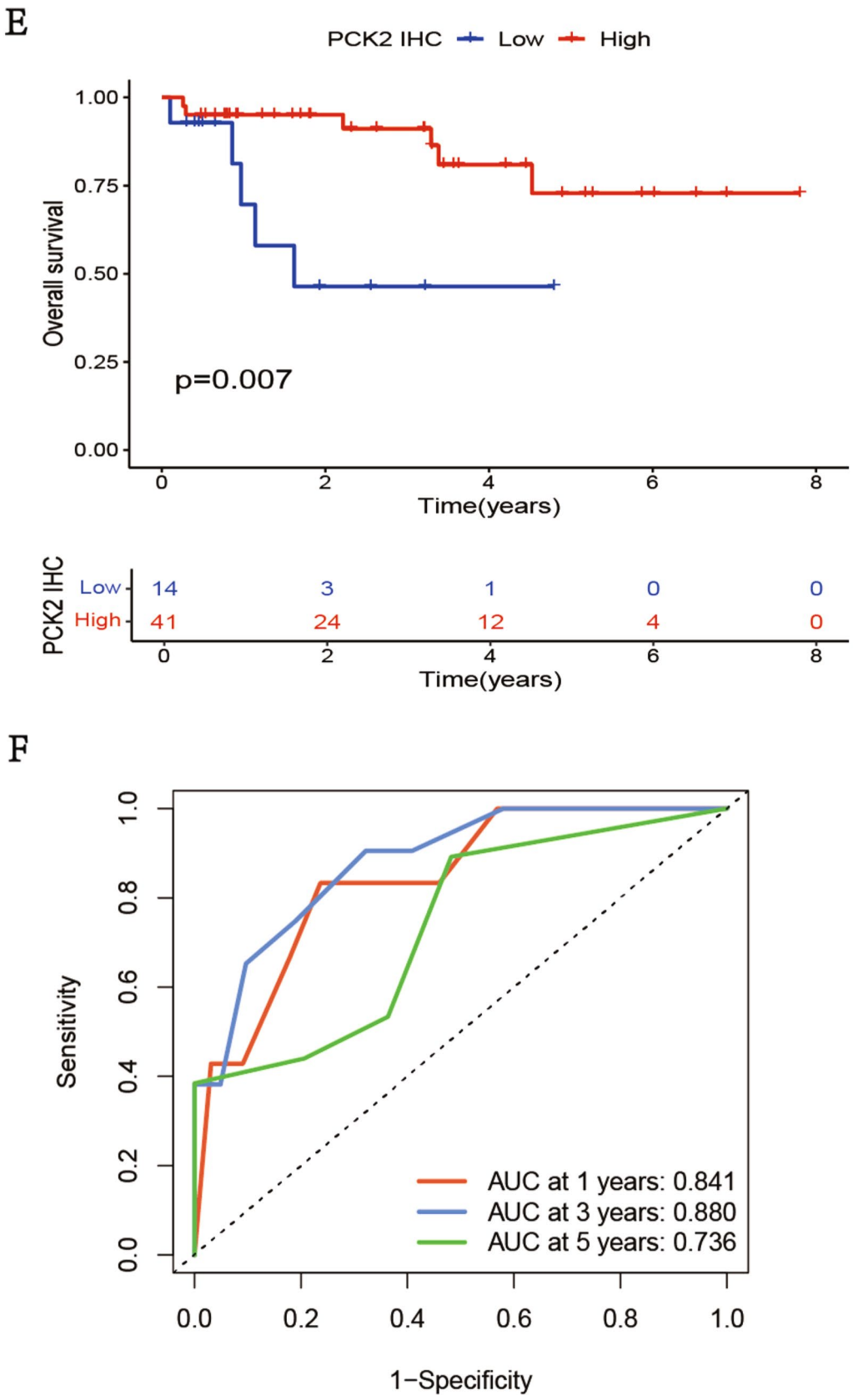

Fig. 4 (continued)

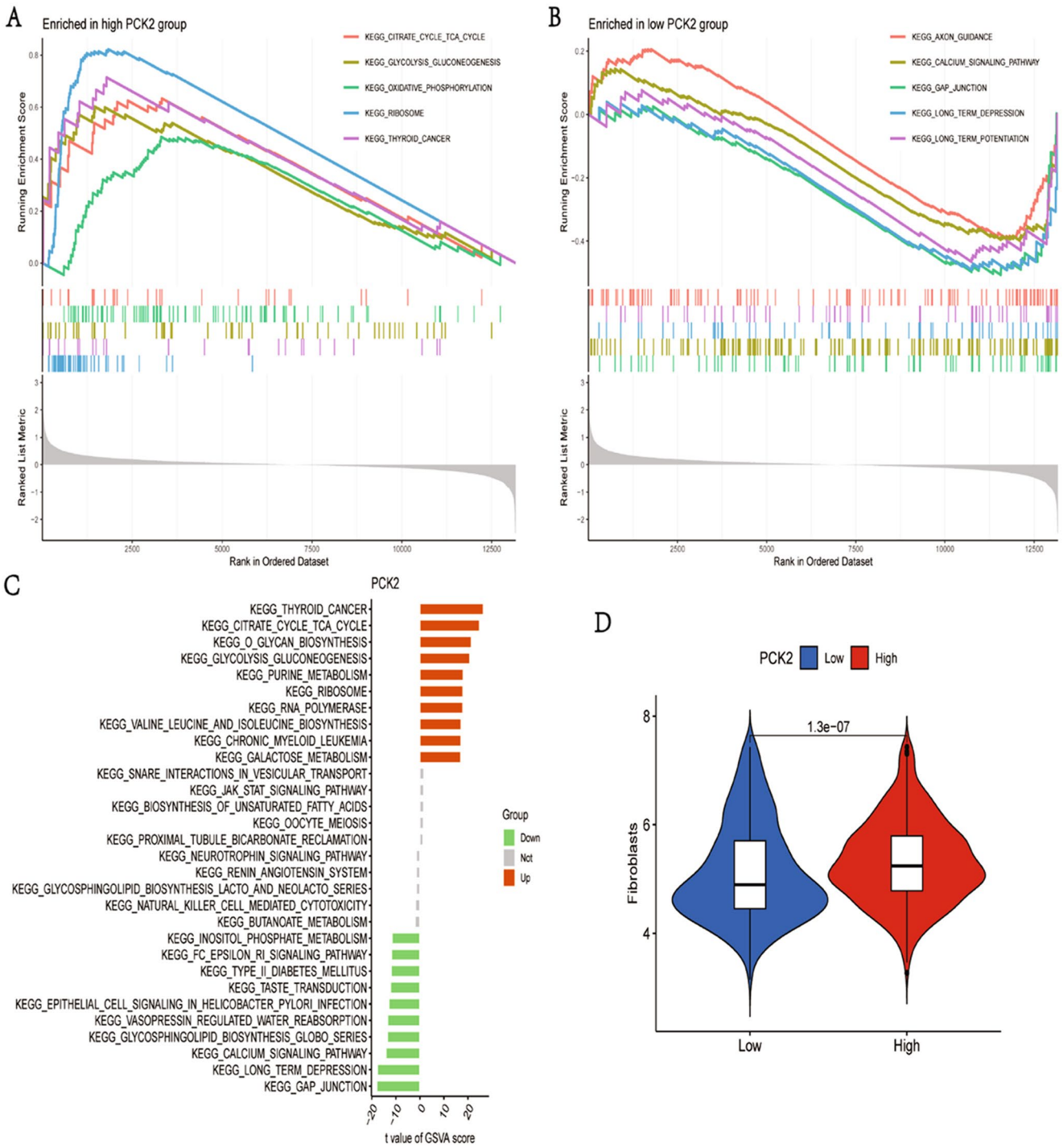

Fig. 5 *PCK2*-related pathways and relationship with the TME in MB. **A**-**B**. Enrichment analysis of high and low *PCK2* expression (GSEA); **C**. Enrichment analysis of *PCK2* (GSVA); **D**-**G**. Immune cell infiltration between different *PCK2* expression groups analyzed by MCP counter, violin plot; **H**. Immune cell infiltration between different *PCK2* expression groups analyzed by CIBERSORT, box plot; **I**. Immune function analysis between different *PCK2* expression groups, box plots; **J**. Correlation between *PCK2* and different immune checkpoints; **H**. Immune cell infiltration between different *PCK2* expression groups by CIBERSORT analysis, box plot; **I**. Immune function analysis between different *PCK2* expression groups, box plot; J. Correlation between *PCK2* and different immune checkpoints; **H**. Immunofluorescence staining of PCK2, CD206 and PD-L1 in MB samples

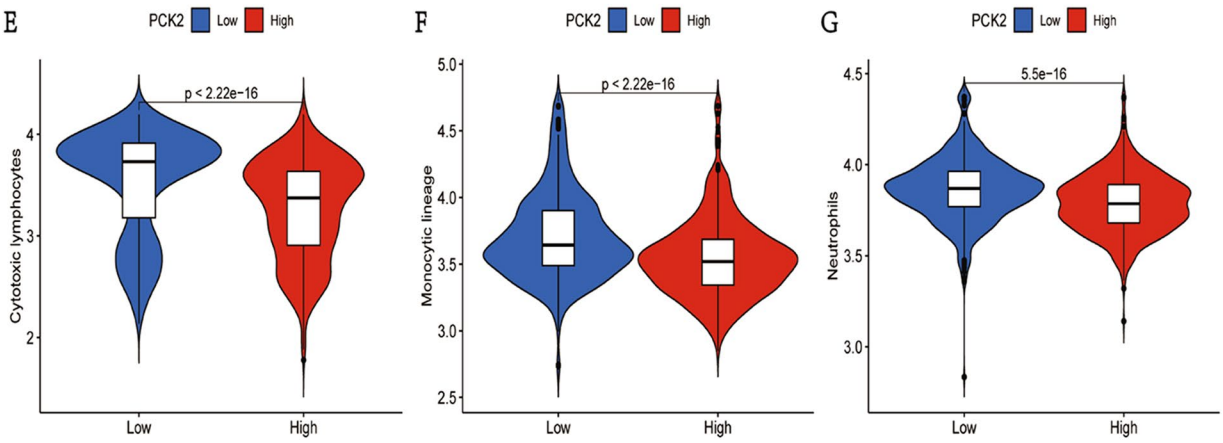

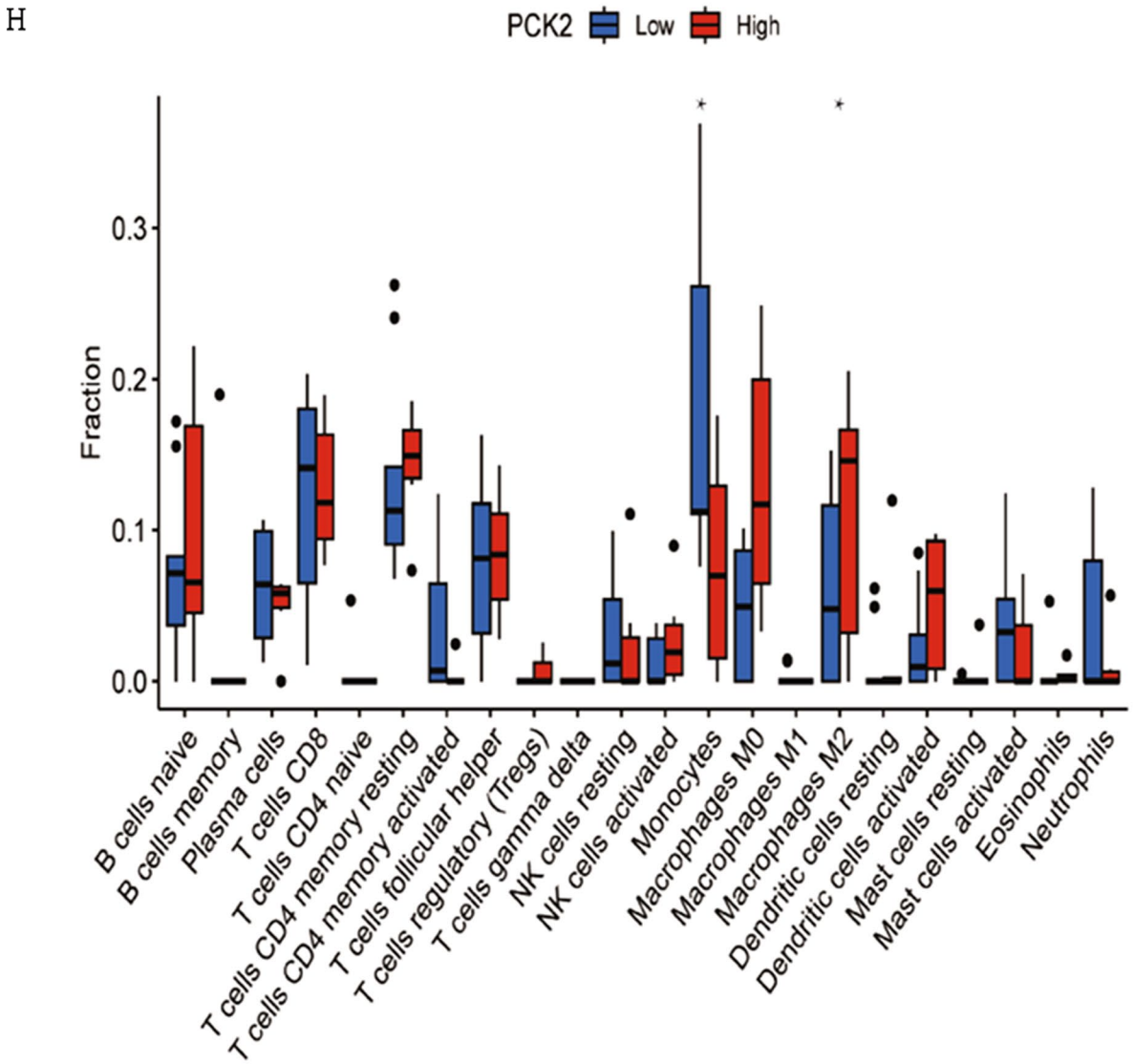

Fig. 5 (continued)

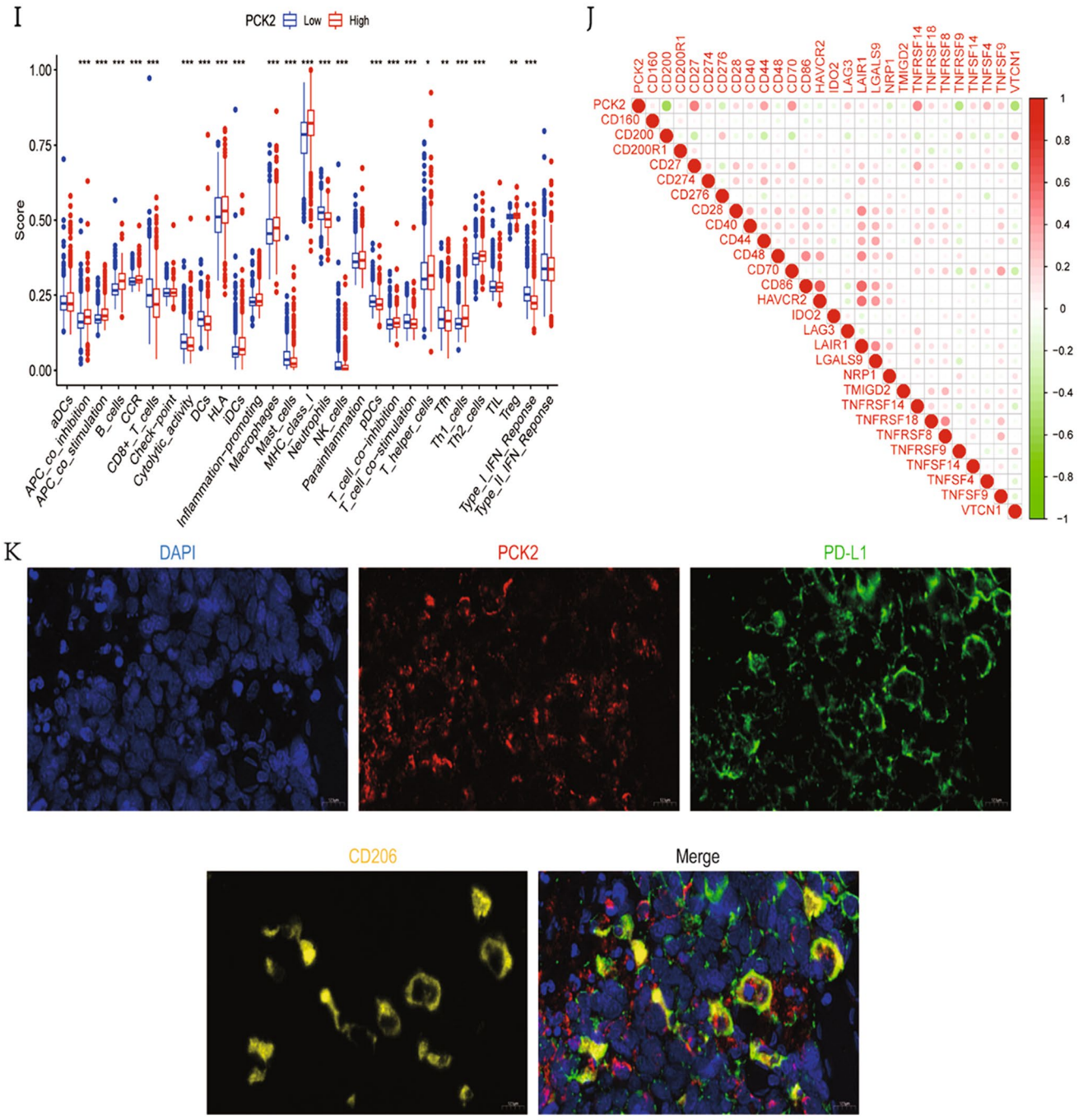

Fig. 5 (continued)

The ssGSEA algorithm was employed to assess the functional activity of immune cells and the enrichment scores of immune-related pathways. In the high *PCK2* expression group of MB patients, there was a significant increase in the activity of macrophages, T cell co-inhibition, antigen-presenting cells (APCs), and B cells, along with chemokine receptors (CCRs), human leukocyte antigens (HLAs), immature dendritic cells (iDCs), MHC class I molecules, T helper cells, Th1 cells, Th2 cells, and regulatory T cells (Tregs). However, in the low *PCK2* expression group, the activities of CD8+T cells, T cell co-stimulation, natural killer cells (NK cells), cytolytic activity, dendritic cells (DCs), mast cells, neutrophils, plasmacytoid dendritic cells (pDCs), follicular helper T cells (Tfh), and type I interferon response were significantly elevated (Fig. 5I).

The correlation analysis between *PCK2* and immune checkpoint genes revealed a significant association between *PCK2* and the expression of several immune checkpoint genes. *PCK2* exhibited a significant positive correlation with *CD274* (*PD-L1*), *CD44* and *LAG3*, while demonstrating a significant negative correlation with *CD86* (Fig. 5J). These findings suggest that *PCK2* may play a role in the immune escape process of MB by modulating the expression of immune checkpoint molecules.

In order to deeply investigate the correlation between *PCK2* and M2-type macrophages and its regulation of the immunosuppression, we randomly selected some samples with high PCK2 IHC score, and systematically detected the expression and localization characteristics of PCK2, M2-type macrophage marker CD206, and immunocheckpoint molecule PD-L1 by multiplex immunofluorescence staining technique. The results showed that PCK2, CD206 and PD-L1 were co-localized in the perinuclear region of the cells (Fig. 5K); correlation analysis further confirmed that PCK2 showed a strong positive correlation with the expression of CD206 ($R = 0.703$), while its correlation with PD-L1 was weak ($R = 0.260$) (Fig. S4).

Discussion

MB is the most common intracranial embryonal tumor in children, and its molecular subtypes serves as the cornerstone for both clinical management and basic research. Currently, IHC markers are widely used to aid in MB molecular subtypes, particularly for the preliminary differentiation of WNT-activated MB, SHH-activated MB, and non-WNT/non-SHH MB. Several markers (β-catenin, GAB1, YAP1, and LEF1) have demonstrated practical value [22, 23]. However, Group 3 MB and Group 4 MB constitute the vast majority of all MB cases and exhibit high heterogeneity in both molecular mechanisms and clinical manifestations. The lack of specific IHC markers complicates the precise subtypes of them [24–26]. Currently, the differentiation between Group 3 MB and Group 4 MB primarily relies on molecular biology techniques, such as DNA methylation profiling. Although these methods offer high accuracy, their high cost and stringent experimental requirements limit clinical adoption and widespread application. Previous studies have explored alternative IHC markers for distinguishing Group 3 MB and Group 4 MB, including NPR3 and KCNA1 [27–29]. However, these markers lack sufficient sensitivity and specificity, restricting their clinical utility. Therefore, to investigate whether biomarkers exist that can effectively distinguish Group 3 MB from Group 4 MB, we employed bioinformatics methods to conduct an in-depth analysis of MB samples from public databases, focusing specifically on Group 3 MB and Group 4 MB subtypes. Our study reveals that the *PCK2* expression significantly differed among MB molecular subtypes and demonstrated an important pathological classification value. Further validation of these findings was conducted using clinical samples from our institution. Results demonstrated markedly elevated *PCK2* expression in Group 3 MB, with comparatively lower expression levels in Group 4 MB. This pronounced expression disparity suggests PCK2 holds potential as a novel IHC marker to aid in the differential diagnosis between Group 3 MB and Group 4 MB.

Phosphoenolpyruvate carboxykinase (PCK) is a key enzyme family in the glycolytic pathway, primarily comprising two isoenzymes: cytoplasmic (PCK1 or PEPCK-C) and mitochondrial (PCK2 or PEPCK-M) [7–9]. This enzyme catalyzes the conversion of oxaloacetate to phosphoenolpyruvate (PEP) within mitochondria, thereby promoting PEP pool formation [13, 14]. Even under glucose-deprived conditions, *PCK2* participates in multiple biosynthetic pathways including serine and glycerol synthesis [30–32]. In tumors, *PCK2* affects tumor cell survival, invasion and treatment response by regulating energy metabolism and oxidative stress : on the one hand, it can enhance tumor resistance to certain drugs (by maintaining energy supply under chemotherapy pressure) [14, 33, 34]. and on the other hand, in renal cell carcinoma, it can increase tumor sensitivity to sunitinib [35]. In some cases, it may aid tumor cell survival and proliferation; in others, it could become a "vulnerability" that renders tumor cells more susceptible to chemotherapeutic agents. This tumor type-dependent dual effect makes its therapeutic application value still unclear, and there is an urgent need to deeply explore the specific mechanism to guide precise treatment.

Our research indicates that high *PCK2* expression is significantly associated in MB with a shortened OS of patients. Multivariate Cox regression confirmed it as an independent prognostic risk factor, with both biomarker and therapeutic target potential. Through GSEA and GSVA analysis, we found that the low *PCK2* expression is closely related to calcium channel signaling. It is speculated that it may affect the cytoplasmic calcium ion concentration by regulating the PEP level, thereby regulating the proliferation, migration and apoptosis of MB cells [36]. However, the specific mechanism of this interaction still needs further verification. Relevant research may provide a new direction for the treatment of MB.

In the TME, nutrient deprivation and molecular signaling can induce immune cell dysfunction and facilitate tumor immune escape [10]. The infiltration behavior of immune cells within tumor tissues influences microenvironmental remodeling and disease progression. Tumors can disrupt immune homeostasis to achieve immune escape, thereby

evading surveillance and attack. Consequently, the state of immune infiltration within the TME plays a crucial role in disease progression, treatment response, and prognostic assessment [37]. M2-type macrophages are the core of the MB immunosuppression by secreting inhibitory cytokines such as IL-10 and TGF-β and expressing PD-L1 inhibit the anti-tumor T-cell response [38, 39]. However, MB immunotherapy is limited by factors such as low tumor mutation burden, insufficient T-cell infiltration, and blood-brain barrier, resulting in poor efficacy [40, 41]. Collectively, these factors constrain the efficacy of immunotherapy in MB, making its treatment a major challenge. Our research indicates that *PCK2* plays a key role in the regulation of the MB microenvironment: High *PCK2* expression is positively correlated with M2 macrophage infiltration and T cell inhibition, and co-expressed with M2 marker CD206 and immune checkpoint PD-L1, suggesting that it may mediate M2 macrophage-related immunosuppression and induce T cell exhaustion or apoptosis by up-regulating PD-L1. Suppress the initiation of immune responses. In addition, PCK2 is co-expressed with CD44 and may synergistically upregulate PD-L1 to maintain the characteristics of tumor stem cells, promote progression and recurrence. The nutrient-sensing pathways and immune-metabolic regulatory networks involving *PCK2* position it as a highly promising therapeutic target [42]. Particularly for Group 3 MB—the subtype with the poorest prognosis—targeting *PCK2* may achieve dual metabolic-immune regulation.

The targeted therapeutic potential of *PCK2* has been verified in various tumors, such as glioma and renal cell carcinoma [12, 43]. At present, *PCK2*-targeting lead compounds such as 3-(3, 4-dihydroxyphenyl)-2-hydroxypropionic acid, 3-mercaptopyridine formic acid and carbazole alkaloids derived from Gardenia jasminoides have been discovered, which have shown tumor-suppressing activity in models of triple-negative breast cancer, liver cancer, etc [44, 45]. Preclinical studies have confirmed that *PCK2* inhibitors or RNA interference can inhibit tumor proliferation, reduce M2 macrophage infiltration and enhance CD8 + T cytotoxicity [38, 39], and their combined use with immune checkpoint inhibitors may produce a synergistic anti-tumor effect, providing a new strategy for advanced or recurrent MB. In addition, the *PCK2*-targeting strategy also holds potential value in areas such as adjuvant chemotherapy for vascular smooth muscle proliferation-related diseases [46]. Current research focuses on the optimization of specific inhibitors, the development of combination treatment regimens, and the exploration of precision treatment biomarkers, providing new ideas for the treatment of malignant tumors including MB.

Our research has involved its own set of limitations. First, the retrospective method of public datasets makes it impossible to include treatment-related variables such as chemotherapy regimens and radiation doses, which may introduce confounding bias; Second, the research results are based on computer simulation analysis and lack functional verification of in vitro (overexpression/knockdown of *PCK2* in MB cell lines) and in vivo xenograft models. Future research will focus on three aspects: (1) Expand the analysis to multi-center datasets containing detailed treatment information to explore the interaction between *PCK2* expression and treatment response; (2) Elucidate the molecular mechanisms by which CRISPR-mediated *PCK2* knockout/overexpression regulates calcium signaling, immune infiltration and therapeutic sensitivity; (3) Explore the efficacy of *PCK2* inhibitors as monotherapy or in combination with immune checkpoint inhibitors in the preclinical model of MB, and develop new treatment strategies for this pediatric brain tumor.

Conclusions

In conclusion, our study sheds light on the multifaceted role of *PCK2* in MB. PCK2 serves not only as a novel IHC marker for differentiating Group 3 MB and Group 4 MB but also as an independent prognostic risk factor and potential therapeutic target. Its function involves dual processes: intrinsic metabolic reprogramming of tumor cells and regulation of the external immune microenvironment. Particularly through its close association with M2 macrophage infiltration and PD-L1 expression, targeting *PCK2* demonstrates broad potential for enhancing the efficacy of MB immunotherapy. These findings underscore the need for further exploration of the mechanisms by which *PCK2* influences M2 macrophage polarization and immune responses. Such an investigation could potentially lead to novel therapeutic strategies for treating MB and enhancing immunotherapy.

Supplementary Information The online version contains supplementary material available at https://doi.org/10.1007/s11060-025-05416-z.

Acknowledgements No.

Author contributions Shiqi Zheng and Long Lin contributed equally. Conceptualization, methodology and writing—original draft preparation, Shiqi Zheng and Long Lin; experimental design, Wenbin Guan and Ruifen Wang; data collection and organization, Guotao Ren, Hangzhu Lan and Yingying Pan; data statistics and summarization, Meng Zhang; writing—review and edting, Lifeng Wang. All authors have read and agreed to the published version of the manuscript.

Funding The authors declare that no funds, grants, or other support were received during the preparation of this manuscript.

Data availability The datasets analysed during the current study are available in the Gene Expression Omnibus database (https://identifiers.org/geo: GSE85217 and https://identifiers.org/geo: GSE37418) and the R2 Genomics Analysis and Visualization Platform (http://r2.amc.nl).

Declarations

Ethical approval All research methods adhered to the Helsinki, the International Code of Ethics for Human Health Research, and other established medical ethics standards and were approved by the Ethics Committee of Xinhua Hospital Affiliated to Shanghai Jiao Tong University School of Medicine (Ethics Approval Number: XHEC-D-2025-181). All research participants provided informed consent during the perioperative period, permitting the use of their identifiable biological samples and clinical data in this study and in future related medical research.

Competing interests The authors declare no competing interests.

References

1. Juraschka K, Taylor MD (2019) Medulloblastoma in the age of molecular subgroups: a review. J Neurosurg Pediatr 24(4):353–363. https://doi.org/10.3171/2019.5.PEDS18381
2. Louis DN, Perry A, Wesseling P, Brat DJ, Cree IA, Figarella-Branger D, Hawkins C, Ng HK, Pfister SM, Reifenberger G, Soffietti R, von Deimling A, Ellison DW (2021) The 2021 WHO classification of tumors of the central nervous system: a summary. Neurooncology 23(8):1231–1251. https://doi.org/10.1093/neuonc/noab106
3. Xiao Y, Ma D, Yang YS, Yang F, Ding JH, Gong Y, Jiang L, Ge LP, Wu SY, Yu Q, Zhang Q, Bertucci F, Sun Q, Hu X, Li DQ, Shao ZM, Jiang YZ (2022) Comprehensive metabolomics expands precision medicine for triple-negative breast cancer. Cell Res 32(5):477–490. https://doi.org/10.1038/s41422-022-00614-0
4. Xiao Y, Yu TJ, Xu Y, Ding R, Wang YP, Jiang YZ, Shao ZM (2023) Emerging therapies in cancer metabolism. Cell Metabol 35(8):1283–1303. https://doi.org/10.1016/j.cmet.2023.07.006
5. Fendt SM (2024) 100 years of the Warburg effect: A cancer metabolism endeavor. Cell 187(15):3824–3828. https://doi.org/10.1016/j.cell.2024.06.026
6. Liang MZ, Huang XF, Zhu JC, Bao JX, Chen CL, Wang XW, Lou YW, Pan YT, Dai YW (2025) A machine learning-based Glycolysis and fatty acid metabolism-related prognostic signature is constructed and identified ACSL5 as a novel marker inhibiting the proliferation of breast cancer. Comput Biol Chem 119:108507. https://doi.org/10.1016/j.compbiolchem.2025.108507
7. Nordlie RC, Lardy HA (1963) Mammalian liver phosphoenolpyruvate Carboxykinase activities [J]. J Biol Chem 238(7):2259–2263
8. Caton PW, Nayuni NK, Murch O, Corder R (2009) Endotoxin induced hyperlactatemia and hypoglycemia is linked to decreased mitochondrial phosphoenolpyruvate Carboxykinase. Life Sci 84(21–22):738–744. https://doi.org/10.1016/j.lfs.2009.02.024
9. Hanson RW (2005) Metabolism in the era of molecular biology. J Biol Chem 280(3):1705–1715. https://doi.org/10.1074/jbc.X400009200
10. Yu Y, Li J, Ren K (2023) Phosphoenolpyruvate carboxykinases as emerging targets in cancer therapy. Front Cell Dev Biology 11:1196226. https://doi.org/10.3389/fcell.2023.1196226
11. Xue S, Cai Y, Liu J, Ji K, Yi P, Long H, Zhang X, Li P, Song Y (2024) Dysregulation of phosphoenolpyruvate Carboxykinase in cancers: A comprehensive analysis. Cell Signal 120:111198. https://doi.org/10.1016/j.cellsig.2024.111198
12. Chen Y, Wang Z, Deng Q, Chen Y, Liang H (2023) Mitochondrial phosphoenolpyruvate Carboxykinase inhibits kidney renal clear cell carcinoma malignant progression, leading to cell energy metabolism imbalance. Am J Cancer Res 13(3):886–899
13. Montal ED, Dewi R, Bhalla K, Ou L, Hwang BJ, Ropell AE, Gordon C, Liu WJ, DeBerardinis RJ, Sudderth J, Twaddel W, Boros LG, Shroyer KR, Duraisamy S, Drapkin R, Powers RS, Rohde JM, Boxer MB, Wong KK, Girnun GD (2015) PEPCK coordinates the regulation of central carbon metabolism to promote. Cancer Cell Growth Mol Cell 60(4):571–583. https://doi.org/10.1016/j.molcel.2015.09.025
14. Vincent EE, Sergushichev A, Griss T, Gingras MC, Samborska B, Ntimbane T, Coelho PP, Blagih J, Raissi TC, Choinière L, Bridon G, Loginicheva E, Flynn BR, Thomas EC, Tavaré JM, Avizonis D, Pause A, Elder DJ, Artyomov MN, Jones RG (2015) Mitochondrial phosphoenolpyruvate Carboxykinase regulates metabolic adaptation and enables Glucose-Independent tumor growth. Mol Cell 60(2):195–207. https://doi.org/10.1016/j.molcel.2015.08.013
15. Lyu G, Li D (2025) ZNF165: A Pan-Cancer biomarker with prognostic and therapeutic potential. Protein Pept Lett 32(3):206–223. https://doi.org/10.2174/0109298665351592250106062250
16. Tian G, Liu C, Che C, Ren S, Zhang K, Zhou P, Wang K, Lu G, Xia Y, Wang Y, Li K, Yang L, Fan X, Wang L (2025) Identifying ARRB2 as a prognostic biomarker and key player in the tumor microenvironment of pancreatic cancer through ScPagwas methodology. Curr Gene Ther. https://doi.org/10.2174/0115665232427614250904061700Advance online publication
17. Lu J, Zhen S, Li X (2025) Characteristics of oxidative Phosphorylation-Related subtypes and construction of a prognostic signature in ovarian cancer. Curr Gene Ther 25(3):327–344. https://doi.org/10.2174/0115665232323373240905104033
18. Wang S, Zhang L, Li D, Gou M (2025) Comprehensive analysis and experimental validation of HEPACAM2 as a potential prognosis biomarker and immunotherapy target in colorectal cancer. Curr Gene Ther 25(4):518–531. https://doi.org/10.2174/0115665232325395241018103006
19. Granat R, Donnellan A, Heflin M, Lyzenga G, Glasscoe M, Parker J, Pierce M, Wang J, Rundle J, Ludwig LG (2021) Clustering analysis methods for GNSS observations: A Data-Driven approach to identifying california's major faults. Earth Space Sci (Hoboken N J) 8(11):e2021EA001680. https://doi.org/10.1029/2021EA001680

20. Mazrouee S, Wang W (2014) FastHap: fast and accurate single individual haplotype reconstruction using fuzzy conflict graphs. Bioinf (Oxford England) 30(17):i371–i378. https://doi.org/10.1093/bioinformatics/btu442
21. Yi L, Jiang C, Guo P, Zhu W, Jiang X (2025) Phosphoenolpyruvate Carboxykinase 2 is a promising prognostic biomarker that correlates with peritumoral dendritic cell infiltration in glioblastoma. J Cancer 16(2):590–602. https://doi.org/10.7150/jca.97034
22. Wang D, Gong J, Zhang H, Liu Y, Sun N, Hao X, Mu K (2022) Immunohistochemical staining of LEF-1 is a useful marker for distinguishing WNT-activated Medulloblastomas. Diagn Pathol 17(1):69. https://doi.org/10.1186/s13000-022-01250-3
23. Aboubakr O, Métais A, Doz F, Saffroy R, Masliah-Planchon J, Hasty L, Beccaria K, Ayrault O, Dufour C, Varlet P, Tauziède-Espariat A (2024) LEF-1 immunohistochemistry, a better diagnostic biomarker than β-catenin for medulloblastoma, WNT-activated subtyping. J Neuropathol Exp Neurol 83(2):136–138. https://doi.org/10.1093/jnen/nlad104
24. Smith KS, Bihannic L, Gudenas BL, Haldipur P, Tao R, Gao Q, Li Y, Aldinger KA, Iskusnykh IY, Chizhikov VV, Scoggins M, Zhang S, Edwards A, Deng M, Glass IA, Overman LM, Millman J, Sjoboen AH, Hadley J, Golser J, Northcott PA (2022). Unified rhombic lip origins of group 3 and group 4 medulloblastoma. Nature. 609(7929):1012–1020. https://doi.org/10.1038/s41586-022-05208-9
25. Ramaswamy V, Taylor MD (2017) Medulloblastoma: from myth to molecular. J Clin Oncology: Official J Am Soc Clin Oncol 35(21):2355–2363. https://doi.org/10.1200/JCO.2017.72.7842
26. Lazow MA, Palmer JD, Fouladi M, Salloum R (2022) Medulloblastoma in the modern era: review of contemporary Trials, molecular Advances, and updates in management. Neurotherapeutics: J Am Soc Experimental Neurother 19(6):1733–1751. https://doi.org/10.1007/s13311-022-01273-0
27. Kim JW, Park SH, Choi SA, Kim SK, Koh EJ, Won JK, Nam SM, Phi JH (2022) Molecular subgrouping of Medulloblastoma in pediatric population using the NanoString assay and comparison with immunohistochemistry methods. BMC Cancer 22(1):1221. https://doi.org/10.1186/s12885-022-10328-6
28. Northcott PA, Korshunov A, Witt H, Hielscher T, Eberhart CG, Mack S, Bouffet E, Clifford SC, Hawkins CE, French P, Rutka JT, Pfister S, Taylor MD (2011) Medulloblastoma comprises four distinct molecular variants. J Clin Oncology: Official J Am Soc Clin Oncol 29(11):1408–1414. https://doi.org/10.1200/JCO.2009.27.4324
29. Shinojima N, Nakamura H, Tasaki M, Kameno K, Anai S, Iyama K, Ando Y, Seto H, Kuratsu J (2014) A patient with Medulloblastoma in its early developmental stage. J Neurosurg Pediatr 14(6):615–620. https://doi.org/10.3171/2014.8.PEDS13590
30. Duplus E, Benelli C, Reis AF, Fouque F, Velho G, Forest C (2003) Expression of phosphoenolpyruvate Carboxykinase gene in human adipose tissue: induction by Rosiglitazone and genetic analyses of the adipocyte-specific region of the promoter in type 2 diabetes. Biochimie 85(12):1257–1264. https://doi.org/10.1016/j.biochi.2003.10.016
31. Devine JH, Eubank DW, Clouthier DE, Tontonoz P, Spiegelman BM, Hammer RE, Beale EG (1999) Adipose expression of the phosphoenolpyruvate Carboxykinase promoter requires peroxisome proliferator-activated receptor gamma and 9-cis-retinoic acid receptor binding to an adipocyte-specific enhancer in vivo. J Biol Chem 274(19):13604–13612. https://doi.org/10.1074/jbc.274.19.13604
32. Beale EG, Forest C, Hammer RE (2003) Regulation of cytosolic phosphoenolpyruvate Carboxykinase gene expression in adipocytes. Biochimie 85(12):1207–1211. https://doi.org/10.1016/j.biochi.2003.10.012
33. Wang SF, Wung CH, Chen MS, Chen CF, Yin PH, Yeh TS, Chang YL, Chou YC, Hung HH, Lee HC (2018) Activated integrated stress response induced by salubrinal promotes cisplatin resistance in human gastric cancer cells via enhanced xCT expression and glutathione biosynthesis. Int J Mol Sci 19(11):3389. https://doi.org/10.3390/ijms19113389
34. Yan T, Zhang N, Liu F, Wang H, Zhang J, Jin X, Jiang S (2024) PCK2 induces gefitinib resistance by suppresses ferroptosis in non-small cell lung cancer. Biochem Biophys Res Commun 723:150200. https://doi.org/10.1016/j.bbrc.2024.150200
35. Xiong Z, Yuan C, Shi J, Xiong W, Huang Y, Xiao W, Yang H, Chen K, Zhang X (2020) Restoring the epigenetically silenced PCK2 suppresses renal cell carcinoma progression and increases sensitivity to Sunitinib by promoting Endoplasmic reticulum stress. Theranostics 10(25):11444–11461. https://doi.org/10.7150/thno.48469
36. Moreno-Felici J, Hyroššová P, Aragó M, Rodríguez-Arévalo S, García-Rovés PM, Escolano C, Perales JC (2019) Phosphoenolpyruvate from Glycolysis and PEPCK regulate cancer cell fate by altering cytosolic Ca2. Cells 9(1):18. https://doi.org/10.3390/cells9010018
37. Eisemann T, Wechsler-Reya RJ (2022) Coming in from the cold: overcoming the hostile immune microenvironment of Medulloblastoma. Genes Dev 36(9–10):514–532. https://doi.org/10.1101/gad.349538.122
38. Tang D, Han B, He C, Xu Y, Liu Z, Wang W, Huang Z, Xiao Z, He F (2024) Electrospun Poly-l-Lactic acid membranes promote M2 macrophage polarization by regulating the PCK2/AMPK/mTOR signaling pathway. Adv Healthc Mater 13(22):e2400481. https://doi.org/10.1002/adhm.202400481
39. Jeroundi N, Roy C, Basset L, Pignon P, Preisser L, Blanchard S, Bocca C, Abadie C, Lalande J, Gueguen N, Mabilleau G, Lenaers G, Moreau A, Copin MC, Tcherkez G, Delneste Y, Couez D, Jeannin P (2024) Glycogenesis and glyconeogenesis from glutamine, lactate and glycerol support human macrophage functions. EMBO Rep 25(12):5383–5407. https://doi.org/10.1038/s44319-024-00278-4
40. Vermeulen JF, Van Hecke W, Adriaansen EJM, Jansen MK, Bouma RG, Hidalgo V, Fisch J, Broekhuizen P, Spliet R, Kool WGM, M., Bovenschen N (2017) Prognostic relevance of tumor-infiltrating lymphocytes and immune checkpoints in pediatric Medulloblastoma. Oncoimmunology 7(3):e1398877. https://doi.org/10.1080/2162402X.2017.1398877
41. Cao L, Xie W, Ma W, Zhao H, Wang J, Liang Z, Tian S, Wang B, Ma J (2023) The unique immune ecosystems in pediatric brain tumors: integrating single-cell and bulk RNA-sequencing. Front Immunol 14:1238684. https://doi.org/10.3389/fimmu.2023.1238684
42. Kim JW, Choi SA, Dan K, Koh EJ, Ha S, Phi JH, Kim KH, Han D, Kim SK (2024) Proteomic profiling of cerebrospinal fluid reveals TKT as a potential biomarker for Medulloblastoma. Sci Rep 14(1):21053. https://doi.org/10.1038/s41598-024-71738-z
43. Lin J, Wu S, Ye S, Papa APD, Yang J, Huang S, Arthur G, Zhuge Q, Zhang Y (2021) Oridonin interrupts cellular bioenergetics to suppress glioma cell growth by down-regulating PCK2. Phytother Res 35(5):2624–2638. https://doi.org/10.1002/ptr.7009
44. Gunasekharan V, Lin HK, Marczyk M, Rios-Hoyo A, Campos GE, Shan NL, Ahmed M, Umlauf S, Gareiss P, Raaisa R, Williams R, Cardone R, Siebel S, Kibbey R, Surovtseva YV, Pusztai L (2024) Phosphoenolpyruvate carboxykinase-2 (PCK2) is a therapeutic target in triple-negative breast cancer. Breast Cancer Res Treat 208(3):657–671. https://doi.org/10.1007/s10549-024-07462-z

45. Long X, Liu R, Zhang M, Wu Y, Zhang S, Tang K, Wang H (2025) Integrated proteomics and phosphoproteomics study reveals the potential tumour suppressive function of PCK2 in hepatocellular carcinoma. Anal Methods: Adv Methods Appl 17(17):3526–3537. https://doi.org/10.1039/d5ay00090d
46. Ko DS, Kang J, Heo HJ, Kim EK, Kim K, Kang JM, Jung Y, Baek SE, Kim YH (2022) Role of PCK2 in the proliferation of vascular smooth muscle cells in neointimal hyperplasia. Int J Biol Sci 18(13):5154–5167. https://doi.org/10.7150/ijbs.75577